UNIVERSIDADE DA BEIRA INTERIOR
Engenharia

A methodology to develop shallow cracks for qualification of a NDT technique

(Versão corrigida após defesa)

Nicole Gomes Dias

Dissertação para obtenção do Grau de Mestre em
Engenharia Aeronáutica
(ciclo de estudos integrado)

Orientador: Prof. Doutor Pedro Vieira Gamboa
Co-orientadores: Prof. Doutor Pedro Miguel Guimarães Pires Moreira
Prof. Doutor Luis Filipe Ferreira Marques Santos
Prof. Doutor Mário Rui Melício Da Conceição

Covilhã, dezembro de 2019

Dedicatory

To my family and in memory of my grandfather

Acknowledgements

I would like to express my immense gratitude to my esteemed supervisor, Dr. Pedro Gamboa for the guidance and patience throughout the realization of this work. My sincere gratitude to Dr. Pedro Moreira for all the knowledge, patience, guidance and hours spent in numerous discussions. To all of the Laboratory of Optics and Experimental Mechanics team, from INEGI, for making me feel welcomed, especially to Benzhad Farahani for having the availability to explain all the important concepts.

It is also with a pleasant feeling that I thank Dr. Luis Santos from OGMA - Indústria Aeronáutica de Portugal, for agreeing to participate in this project since an early stage and following it with care. His experience in the maintenance field gave me a realistic context of how procedures are done. A thank you as well to Dr. Rui Melicio, from University of Évora, for all the words of encouragement and dedication demonstrated along the realization of this dissertation.

My acknowledgements are also going to Dr. Nuno Correia, Technician Andreia Durães and Engineer Ricardo Pinto for the availability to receive me in the beginning of this project.

To my friends that always encouraged me and especially to Pedro, that without hesitations and with kind words, helped me during each step of the way.
Lastly, I would like to take this opportunity to express my gratitude to my family who always inspired me and believed in me. Without them, nothing of this would be possible.

Resumo

Inspeções e manutenções são processos importantes na indústria aeronáutica. Os processos sofreram uma evolução significante ao longo dos anos devido ao forte desenvolvimento das frotas aeronáuticas. Para garantir a segurança da aeronave, todos os danos críticos devem ser intercetados no tempo devido antes de se tornarem danos irreversíveis que comprometam toda a estrutura.

Nesta dissertação foi desenvolvida uma metodologia para criar fendas de fadiga de uma certa dimensão para serem usadas na qualificação de processos de inspeção não destrutivos. A metodologia foi desenvolvida tendo por base métodos numéricos, trabalhando com provetes de espessura de $2mm$ com entalhe pré-existente. Para a qualificação dos processos de inspeção não destrutivos, o objetivo passou por criar uma fenda de fadiga não penetrante no provete. Um teste de flexão a quatro pontos foi modelado para restringir a direção da propagação da fenda em espessura. Abaqus®, um *software* de modelação de elementos finitos, é também usado para determinar o fator de intensidade de tensão ao longo da propagação da fenda, seguida de uma abordagem matemática usando a lei de Paris é também apresentado para determinar a propagação da fenda com o número de ciclos. Usando o *software* NASGRO® foi possível determinar o número de ciclos de fadiga que são necessários para que uma fenda iniciada no entalhe inicial se propague até à dimensão pretendida.

Os resultados obtidos indicam que o teste de flexão a quatro pontos é uma escolha apropriada para criar a fenda com as dimensões impostas. Com o uso do software de modelação de elementos finitos, foi observado que o fator de intensidade de tensão é maior na fenda final e assume o menor valor para a fenda inicial. Com os valores do fator de intensidade de tensão, foi feito um estudo de verificação dos valores no domínio da Lei de Paris. Uma relação entre os ciclos de fadiga e os valores do fator de intensidade de tensão foi alcançada, significando que, com o aumento dos ciclos de fadiga e os valores do fator de intensidade de tensão também aumenta e consequentemente, a fenda tende a desenvolver ao longo da espessura do provete.

Palavras-chave

Fendas, ciclos de fadiga, fator de intensidade de tensão, Lei de Paris

Abstract

Inspection and maintenance are important processes in the aeronautical field. The processes suffered a significant evolution over the years, due to the strong development and growth of aeronautical fleets. To guarantee aircraft safety, all critical damage should be intercepted in due time before it become an irreversible damage and compromise the entire structure.
In this dissertation a methodology to create fatigue cracks of a certain dimension to be used on the qualification of NDT processes was developed. The methodology was developed based on numerical approaches, working with $2mm$ thick cracked specimens. For the qualification of the NDT process, the objective was to create a shallow fatigue crack on a specimen. A four-point bending test was modelled to restrain the crack propagation direction through thickness. Abaqus®, a finite element method software, is used to determine the stress intensity factor along the crack propagation, followed by a mathematical approach using Paris Law which is also presented to determine the crack growth along with the number of cycles. Using the software NASGRO® it was possible to determine the number of fatigue cycles that are needed for a crack starting at the initial notch to achieve the desired dimensions.
The results portrayed indicate that the four-point bending test is an appropriate choice to create the crack with the imposed dimensions. By the use of the finite element method software, it is observed that the stress intensity factor is higher in the crack tip and it assumes the lower value in the notch tip. With the values of stress intensity factor, a verification study of the values was made in the Paris Law domain. A relation between the number of fatigue cycles and the values of stress intensity factor was achieved, meaning that, with the increase of fatigue cycles, the stress intensity factor also increases and consequently, the crack tends to develop into the thickness specimen.

Keywords

Crack, fatigue cycles, stress intensity factor, Paris Law

Contents

List of Figures

List of Tables

Nomenclature

Symbols	Description	Units
K	Stress-intensity factor	$MPa\sqrt{mm}$
K_c	Fracture toughness or Critical stress intensity factor	$MPa\sqrt{mm}$
K_{Ic}	Plane strain fracture toughness	$MPa\sqrt{mm}$
K_t	Theoretical elastic stress concentration factor	$MPa\sqrt{mm}$
K_σ	Geometrical mean of the stress concentration factors	$MPa\sqrt{mm}$
K_ε	Geometrical mean of the strain concentration factors	$MPa\sqrt{mm}$
ΔK	Stress intensity factor range	$MPa\sqrt{mm}$
k_t	Stress concentration factor	$[-]$
N	Number of applied fatigue cycles to failure	$unit$
n	Number of cycles	$unit$
a	Crack propagation distance	mm
b	Crack height	mm
c	Transversal crack size (relative to a)	mm
G	Energy release rate for linear material	N/mm
J	Energy release rate for nonlinear materials	N/mm
δ	Crack-Tip Opening Displacement	mm
f	Newman's crack opening	$[-]$
R	Stress ratio	$[-]$
S_f	Fatigue limit of the material	MPa
σ	Nominal stress	MPa
σ_A	Stress concentration	MPa
σ_0	Yield strength	MPa
τ	Shear stress	MPa
ε	Strain	$[-]$
ν	Poisson's Ratio	$[-]$
V	Shear force	N
M	Bending moment	Nmm
E	Young's Modulus	GPa
P	Load	N
L	Beam length	mm
I	Area moment of inertia	mm^4
W	Width	mm
t	Thickness	mm
B	Crack offset	mm
$S0$	Tension/compression stress	MPa
$S1$	Bending stress in the thickness	MPa
e	Distance from neutral axis to edge	mm
T	Short transverse direction	$[-]$
U	Crack closure function	$[-]$
μ	Shear modulus	MPa

Subscripts

max	Maximum
min	Minimum
x	Component along the x-axis
y	Component along the y-axis
z	Component along the z-axis
th	Threshold
eff	Effective
op	Opening

List of Acronyms

AA	Aluminum Association
ASTM	American Society for Testing and Materials
CCD	Charge-Coupled Device
CVM	Comparative Vacuum Monitoring
CTDO	Crack-Tip Opening Displacement
DPHM	Diagnostics, Prognostics and Health Management
EDM	Electro Discharge Machined
EPFM	Elastic-Plastic Fracture Mechanics
FEM	Finite Element Method
GAG	Ground-Air-Ground
LEFM	Linear Elastic Fracture Mechanics
MT	Middle-Tension
NASA	National Aeronautics and Space Administration
NDE	Non-Destructive Evaluation
NDI	Non-Destructive inspection
NDT	Non-Destructive Test
NMR	Nuclear Magnetic Resonance
PVDF	Polyvenylidenfluorid
QNDE	Quantitative Non-Destructive Evaluation
SHM	Structural Health Monitoring
SQUID	Superconducting Quantum Interference Device

Chapter 1

Introduction

Over the years, several aircraft structural models have been developed. Structural design progressed and some structures caused more impact than others, such as the wire braced structures, built until 1930, with biplanes and using wood as its main component. Later, these evolved to monoplane and metallic construction. Mainly, began to use truss type construction as support links along the aircraft interior to keep its form [12]. Posteriorly, came the semi-monocoque structures where the structure was stronger and allowed the possibility to renounce internal supports and increase the space available. This type of construction allowed aircraft to increase the pressurization loads which in turn increased the operation ceiling. Nowadays, this type of structure is still in use where the fuselage is reinforced with lengthwise longerons and stringers and crosswise frames while the wing internal structure has spanwise spars and stringers and chordwise ribs [12]. By looking into the future and having a historical based structural evolution in mind, it was possible to achieve a structure that assures suitable properties for the aircraft. Isogrid Structure serves as an example, which is designed with reinforcements in regular triangular patterns conceiving a giant network with high damage tolerance that can be applied to composite materials [13]. This structure main focus is aerospace with a future perspective to be applied to commercial and military aircraft. Considering all this structural evolution and achieving all this air dominance, aviation became a study for high safety standards. The aircraft structure, as any mechanical component, is subjected to all kind of stresses, either external or internal, and these aerodynamic forces, as pressurisation or mechanic stresses which deteriorate the structures, could lead them to possible irreparable flaws if not detected in time.

Nowadays, safety is a major concern to all aircraft operators, thus any type of possible damage should be detected as soon as possible. This action has a high importance, as it can save material, components and increase safety. In an economic way, the aircraft industry tries to lower repair and maintenance expenses, so there is a commitment to try to identify all damage in regular inspections and fix the component while the repair procedure is considerably simpler. To avoid a worst-case scenario, any damage that begins in an aircraft component could evolve to a possible failure. An unpredicted and undetected fracture is a serious problem in the aviation industry, thus a very important field comes into place to try to understand and predict fracture - Fracture Mechanics.

Fracture Mechanics is a discipline that studies the material behaviour in the presence of a crack. Many factors could make a small crack or defect to appear in a structure, where the environment and incorrect or inappropriate design are typically the main factors. The first evidence of fracture mechanics application was in the Second World War, in 1941, in the Liberty Ships. These ships were revolutionary for its time: they were the first to have all welded hulls, which improved time production relatively to riveted designs. However, the material did not change. In the riveted design, fracture did not propagate across the riveted panels, opposite to a welded structure where, as a single piece, the fracture propagated without any constraints [4]. The material was also not prepared to handle specific temperature ranges: when the ships needed to navigate to low temperature zones, the material that was ductile, displaying a brittle behaviour. This had devastating consequences, as the ship split in two. A crack presented in a brittle

material is far more dangerous that in a ductile one, because in the brittle material the crack grows with a very small plastic deformation, and without any resistance a fracture is easily created. However, in a ductile material, the material will experience plastic deformation, which delays crack initiation and propagation [4].

1.1 Motivation

Worldwide, aircraft are considered the safest and most efficient means of transportation. In order to obtain those results, several safety protocols have been employed with the intent of increasing safety. Starting with the initial design of the aircraft, where several engineering concepts and philosophies are implemented as Fail Safe, a practice performed to contain any structural flaw and its damage to be minimal; Segregation, requirements that assure the components have been produced or maintained properly, if they did not, segregate those parts of questionable nature from serviceable parts [14]; as well as Damage Tolerance, that can be evidenced when an existing flaw has the ability to hold on until its repair. All design philosophies referred above need constant monitorization of the aircraft condition, which is required for damage prevention and therefore avoiding catastrophic failures, such as aircraft loss. These philosophies indeed increase the safety by the early detection of structural damage.

SHM (Structural Health Monitoring) is a powerful tool that revolutionized the inspections and maintenance procedures and it can, in a schedule way, monitor critical structural degradation and provide an economical advantage, on account of being more viable to repair the damage in an early stage. Its concept is based on non-destructive methods of structural analysis, which aims to anticipate and permanently monitoring the structure in order to find flaws or any other kind of structural damage. A neural network of sensors, processors and computers are used to achieve the purposes of SHM. For inspection and Damage Assessment purposes, there is no need for structure disassembling, saving a considerable amount of time and cost to operators. Boeing [15] concluded that 85% of maintenance effort is spent on tearing down and re-assembling the components and only 15% of work is spent on actual inspection. SHM is inserted in a procedure group of Non-Destructive Testing which defends that all procedures should be performed trying to accomplish the least amount of damage on the structure. Some examples of these procedures are already in use by aeronautical companies, such as ultrasonic waves, X-rays, thermography, liquid penetrant tests and eddy currents. Some of these technologies, as for example ultrasonic waves and eddy currents, will allow remote damage assessments, damage detection, damage evaluation and damage continuing monitoring. These procedures can be fully automated or can be manual or programmed for every scheduled maintenance. These types of technologies will also enhance the possibility of performing the inspections without having full access to the structure, i.e., the aircraft or specific part/area does not need to be fully disassembled to perform these tests/inspections, reducing the aircraft maintenance time and costs. One of the most defying challenges is to detect the structural problems in its beginning. Referring to Subsection 2.2, Figure 2.3, Lourenço [3] objective is to develop tools to detect the damages at the Micro Crack Growth phase. The advantages are obvious; the first is safety, an early detected problem decreases the probability of a catastrophic event. The second is economic, an early detected damage have less repair man hours and material needs; it also prevents post economic issues such as delayed or cancelled flights.

Other big challenge is regulations. The current regulatory background does not predict that inspections can be carried out remotely or indirectly without human intervention. Aircraft

manufacturers must develop these procedures only when these types of technologies are reliable enough to detect 100% of the damages. The aviation authorities must approve these types of technologies and inspections in order for those to be adopted by the industries.
Since a boost on inspection methodologies is a constant demand by aircraft maintenance engineering, new technologies for NDT (Non-Destructive Testing) must be developed. This development, demands the use of specimens with known fatigue cracks, replicating real aircraft parts. The development of such specimens imposes the research on methodologies for their manufacturing.

1.2 Objectives

Since inspection and maintenance procedures should be continuously developed based on fracture mechanics based knowledge, the main goal of this dissertation is the development of a methodology to manufacture specimens with known fatigue crack geometry that can be later-on used for qualification of new NDT techniques. This thesis is based on numerical studies for the manufacture of shallow cracks.
The determination of the stress intensity factor along the crack propagation, as well as, the determination of the number of cycles that should be applied to a specimen with an initial EDM (Electro Discharge Machined) notch until it evolves to a fatigue shallow crack of established dimensions are presented as main objectives. Another main goal is to provide a link between the numerical study and mathematical concepts, giving a relation between the crack dimension and the number of cycles from the retrieved data. The numerical work developed on this thesis is a first and important step that should be later validated through experimental testing. The third step, shall be the qualification of new NDT techniques which will be able to detect the manufactured defects (fatigue cracks).

1.3 Layout of the Dissertation

The dissertation is organized in five chapters. The first chapter contains an introduction with its respective motivation and objectives.
The second chapter is the literature review, where the theoretical concepts are briefly explained.
A theoretical and mathematical background is presented for the four-point bending fatigue test in the third chapter. Here, the principal foundations for the following chapter are explained.
In the fourth chapter, the numerical configuration and the respective results obtained by the used software are presented. A discussion of the results is also presented.
The last chapter is dedicated to conclusions. The achievements and some suggestions to future work are presented.

Chapter 2

Literature Review

In the current chapter a literature survey of the topics to be addressed in this document is performed. The most important theoretical aspects are highlighted and an overview is presented.

Inspections and maintenance requested by aircraft operators are an important step to guarantee aircraft safety and airworthiness. Many inspection methods are being implemented and every day some new ideas for non-destructive evaluation and new inspection techniques appear.

However, during maintenance tasks some defects are not detected. Some punctual defects that could possess a high probability of becoming a dangerous damage, can sometimes be mistaken by others, with a lower level of importance and risk. Most times, only experienced technicians are capable of noticing the differences and proceed accordingly. Fatigue loading and its implications are of great importance to aircraft's manufacturers, and they represent one possible case of defects that go unnoticed.

In the first section, Structural Health Monitoring is approached and it is followed with a small historical overview, as well as its benefits for aviation industry.

In the second section of this chapter, an approach of fatigue failure and its importance in the aircraft industry is made.

A historical evolution of the fatigue damage is addressed, as well as several study possibilities for trying to detect and understand this phenomenon in the materials.

In the third section, an introduction to fracture mechanics is made with its main focus lying on its theories and principles. Firstly, it is discussed the LEFM (Linear Elastic Fracture Mechanics) followed by a brief reference to EPFM (Elasto-Plastic Fracture Mechanics).

2.1 Health Monitoring

SHM is a set of structural analysis method that arose with the evolution of convectional tests whose primary goal is to perform a non-destructive structural inspection. Cracks or any other types of damage present in the structure, that can become critical and compromise all the aircraft structural integrity, can be detected with SHM. This program displays two possible action strands, with one performing real-time monitoring whilst the other performs when the inspections are programmed. According to Peter Foote [16] 'SHM is an emerging technology and has a long history of research and development. The needs of the aerospace industry to maintain and assure the integrity of safety critical airframes have provided a driver for this development'. Added by Keulen *et al* [17] this is a technique that performs permanent monitoring of structural damage, assuring operational low time consumption and also offering a higher rentability and performance in structural maintenance. High cost and many hours of work due to the inspections complexity by removing access panels to inspect the components, could be replaced by SHM, resulting in financial compensation and less wasted time.

2.1.1 Aircraft Non-Destructive Evaluation

Aircraft NDE (Non-Destructive Evaluation) is a SHM powerful tool that has been gaining a lot of recognition in the aircraft community. It is defined as a set of inspections, tests and evaluations of materials, components and systems in search of discontinuities before they cause severe damage, operation inefficiencies, or in-service failures [18]. The diagnosis and prognosis of damage are the key-point of SHM or maintenance-based conditions, with high dependence of time and action, maintaining the damage in the acceptable thresholds. From a business perspective, EMBRAER [19], [20] defines SHM, as well as Achenbach [21] with QNDE (Quantitative Non-Destructive Evaluation), for being a material characterization method and a path to access the flaws of the structural component, with the purpose to understand the elastodynamics behaviour of the ultrasonic waves in the material and it could be done in components that are critical or their maintenance costs are expensive, reducing human-factors during inspections. Alike Worden, Manson and Allman [22] classified the non-detection problem in four levels, denominated as Detection, Localization, Assessment and Prediction respectively, where three different algorithms are applied: Kernel density estimation, Outlier analysis and the neural network. Wölfinger *et al.* [23] approached this problem using piezoelectric transducers as a detection method made of PVDF (Polyvenylidenfluorid), that is a piezoelectric plastic material and when it is mechanically deformed it generates a charge, or ceramic blades, where their signal analysis could bring information associated to the destructive or non-destructive effects, the damage extension and the impact point location. Aside from visual inspection, the conventional non-destructive methods such as ultrasonic, X-rays, thermography and eddy currents can be adopted for damage detection [24] in the aircraft structure for signs of corrosion, fractures and cracks. NDE as technique evolved with the passage of time, and in 2008 was presented by QI *et al.* based on advanced sensor techniques such as [25] 'Ultrasonic testing with piezoceramic sensor arrays, air-coupled transducers, and dry-coupled transducers, Eddy current testing with SQUID (Superconducting Quantum Interference Device) magnetometer sensors, Hall effect sensors, and giant magnetoresistive sensors, optical testing techniques including thermography with infrared sensors, laser shearography with CCD (Charge-Coupled Device) sensors and other NDE methods including microwave testing with waveguide sensors, vibration monitoring with fiber optic sensors, and magnetic resonance testing with NMR (Nuclear Magnetic Resonance) sensors'. In spite of NDE advantages, these methods have two major limitations. Zhao, X *et al.* [15], in 2004, stated that 'the NDE inspections had to be done on ground', when the optimal perspective was to continuously monitor the aircraft structure state, both in ground as in flight, and the 'equipment for NDE is bulky', it would be necessary small and light sensors and equipment capable of controlling the structure data at all time [15]. Starting with ultrasonic testing that is used to locate external and internal material defects and it is based on short, high frequency sound pulse waves. When a defect is detected, it tends to reflect part of the energy of the sound wave, and it will be shown a wave discontinuity on the screen [18]. The Eddy current method is commonly used in the aeronautic industry for being a simple NDE with great surface detection capabilities provided with electromagnetic induction. When an alternating current is applied in a coil, a magnetic field is created. With the proximity of an electrically conductive material, eddy current is induced in the material and it is variable in accordance of the alternating current variations. Therefore, when a discontinuity is found, the magnetic field is changed and a defect signal can be read by measuring the coil impedance variation [26]. Thermography and laser shearography are two examples of optical testing. The first one, allows to see temperature variations that can be indicative of weakness in the material. Infrared cam-

eras are used for this type of NDE in order to give electrical, mechanical, thickness and general flaw information [18], as it can be used in all kind of material geometries and combinations [27]. Laser shearography requires the stressing of the component surface, and this can be done by heat, vacuum or vibration excitation [28]. This technique has the capability to detect the range of damage in several kinds of geometry types, and its operation is based on the capture of two images with the first one being an image of the surface in a neutral state, and the second representing the surface under stress. The comparison between the images quickly identifies variations among both images revealing underlying issues [18]. According to Mrad [29] a more recent approach has been studied – DPHM (Diagnostics, Prognostics and Health Management). The principle of this concept is to be a 'central information system on-line collaborative environment in aircraft autonomic logistics' [29], meaning that this system can provide diagnosis if the components are able to perform its functions. It also gives a prognosis, a prediction tool to provide advice and a possible outcome for the component, and for Health Management this system reports a decision based on the previous two recognition phases, that accounts for available resources and operational demand. This tool has shown good results in predicting failure with high accuracy and high confidence. Another type of NDE that has been in development with promising results in specific cases are CVM (Comparative Vacuum Monitoring) and the techniques applied to Lamb Waves. Using Rulli and Dotta's definitions [1] 'The Comparative Vacuum Monitoring (CVM) technology is based on the principle that a vacuum maintained within a small constant volume is extremely sensitive to any leakage' [1], by using air and vacuum in independent pipes with specific constant pressures that it can change when some kind of damage induce the leakage. Lamb waves, discovered by Horace Lamb in 1917, were presented with great benefits to damage detection with low maintenance costs and low energy consumption, and it is capable of pinpointing the location and form of the damage. They are generated at one point, travelling through the thickness of the component and presenting the ability of scanning even the internal defects and cross vast distances in both surfaces. This promising tool has been subjected to several tests. In 1992, David Alleyne and Peter Cawley [30] proceeded to classify Lamb Waves using the method of finite elements and Fourier's Transform as the theoretical fundaments. The ambition of these tests was to rate the sensibility of wave symmetric modes S_0 and wave asymmetric modes A_1 and A_0, represented in Figure 2.1.

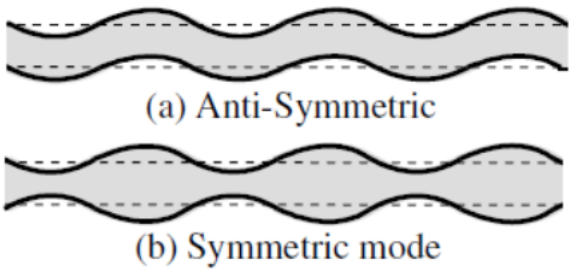

Figure 2.1: Lamb Waves representation [1].

The use of A_0 and S_0 modes were due its easy generation and detection, and S_1 modes were used in zones with very dispersion since this characteristic is common in other modes. Besides the damage detection, this kind of technology could also display the damage size. EMBRAER added that 'the fundamental of this technique is based on the assumption that structural damage changes the physical dynamic response of the structure, such as natural frequencies, mode shapes and damping, frequency response, etc' [1]. To perform all these NDE methods, the most

important components are the sensors. The sensors are the tools capable of receiving and, sometimes, send the information necessary to analyse the damage detection in the different techniques. There are numerous types of sensors, with different types of capacities and abilities built with different materials and geometries that can adapt to many circumstances of work. The smart sensors are one type of sensors that fulfil the objective of a traditional sensor, furthermore it has the advantage of self-testing that can have a great impact to its implementation, providing easy maintenance and increased viability. A more accurate definition is given by Beeby, P *et al.* [31] 'The integration of sensor and electronics allows it to be treated as a module, or black-box, where the internal complexities of the sensor are kept remote from the host system. Smart sensors may also have additional integrated sensors to monitor, say, localized temperature changes. This is sometimes referred to as the sensor within-a-sensor approach and is an important feature of smart sensor technology' [31]. Tested by Zhao, X. *et al.* [15], there are two ways of NDE implementation: wired and wireless. The most traditional is wired, but implies a lot of wires connected, and if live-monitoring was the final goal, it would imply an increase in aircraft weight, so in alternative, they studied the wireless option, where they used antennas, transducers and sensors, and the technique showed a lot of potential for monitoring the crack growth [15].

2.2 Fatigue Failure

Fatigue has been a structure problem for the structural designers for many years. For being an important, unpredictable and not-warning failure, a lot of experimentation was made in order to find new materials with high fatigue tolerance and to try to avoid errors that can compromise the safety. A long list of aircraft historical accidents due to fatigue problems has been recorded, and it is a guided book that all regulated entities and operators have been following. A definition given by Bruhn [32] 'Fatigue failure is failure due to being stressed a number of times'. This concept is perhaps the simplest and most direct definition, however in a more technical perspective, Bruhn [32] described that a 'Fatigue failure appears to begin with a crack starting at a point of weakness in the material and progressing along crystal boundaries', meaning that a small crack start tends to propagate through the material when an action is repeated several times creating a stress cycle causing structural failure.
In 2017, Habib, S. *et al.* [33] defined fatigue as 'fatigue is based upon repetitive loading below the yield stress which can lead to premature failure', and completed that it was several types of fatigue, as high-cycle, low-cycle, thermal, surface, impact, corrosion and fretting. Katifes, X. [2] follows the same definition as previous authors, that fatigue failures begin with a form of crack that propagates through the structure until it is no longer a safe structure or it causes a structural failure. Cyclic loads that an aircraft is subjected has the consequence of some failure cracking. In Figure 2.2 is shown a GAG (Ground-Air-Ground) loading that a commercial aircraft has to endure at each step of flight.

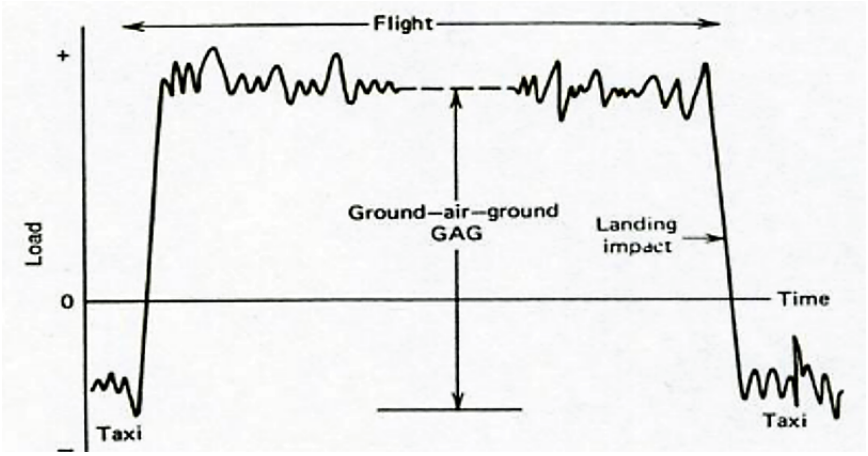

Figure 2.2: GAG wing loading of a Commercial Aircraft [2].

As it can be seen, the take-off and landing present an abrupt range of loads, and during flight these loads have several changes over time. These cyclic loads occur every time that an aircraft fly, and other factors as temperature, environmental conditions, microstructure voids contribute to cracking fatigue step in.
Many investigations over the years were done to understand fatigue behaviour, in either metals or alloys, but fatigue cracking is still the most common cause of aircraft failure, and they occur from unexpected conditions [2].
The structure accountable to a fatigue crack follow three stages [2]:

1. Initiation of fatigue crack;
2. Propagation, only depends on the material;
3. Failure, the material achieves the limit of loads support.

These stages could be seen in more detail in Figure 2.3.

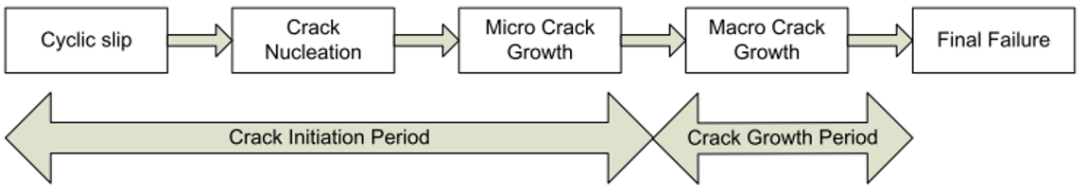

Figure 2.3: Crack Failure Propagation [3].

According to Bruhn's fatigue failure definition [32], micro crack growth is related to the material crystal structure. In the case of macro crack growth and after analyzing a flawed component, it can be seen as beach marks. These macroscopic marks, are surface marks that a fatigue crack leaves on the surface before reaching failure, which tends to be a smooth surface near the origin of the crack and rougher as the crack progresses [2].
The catastrophic consequence that a failure could deliver in a service aircraft reflects in a common concern and efforts to try to prevent all the possible disasters that could occur due to fatigue, or other type of structural damage. One way is to seek how different materials behave

with several circumstances of load, geometry and location along the aircraft, and herewith to study how troubles from different types of structural failure could be avoided. In this line of thought, NDI (Non-Destructive Inspections) have shown great importance, finding possible damages and preventing both incidents and accidents. As was mentioned before, has been subject to change through history.

According to Bruhn [32], in 1973, fatigue testing could be done with 3 types of tests:

1. Material Crystals

2. Small Structural Test Specimens

3. Complete Composite Structures.

The first one was done in a microscopic way, analysing the crystals of the material and determining if there was a propagation along the boundaries of a small crack; a lot of tests information are available on the second one. The third test is an innovative technique that has risen from testing complete structure units, as a complete wing or fuselage, evolving to a full-scale structure, the airplane.

In 1976, Payne [34] believed the better way to inspect fatigue failures was to perform a full-scale structure fatigue test. This technique consists in identifying the different loads that the aircraft is subjected in its operating flight, simulating these loads in an aircraft and thereafter, performing a full load history in order to find the fatigue spots with increased accuracy. However, this approach encountered some difficulties, such as:

- Predicting the fatigue in a complex structure from only having basic or generalised fatigue data in cyclic loading conditions;

- Without knowing the cracks propagation, trying to establish a reliable inspection procedure to ensure detection of it.

The different loads applied should be as close as possible to reality and should include flight by flight loads, that consist in gust, manoeuvre, pressurisation, taxing, take-off and landing loads. To demonstrate a more realistic test for different aircrafts, loads should depend on the flight envelope [34].

Experimental cases, as flexural fatigue, are the best way to test and simulate fatigue. By knowing which parameters guided the fatigue behaviour, D'Amore et al [35] applied a four-point bending test to simulate fatigue behaviour with different stress ratio, that is the ratio of the minimum to the maximum applied stress, and concluded that this particular ratio is a primordial parameter of fatigue. Joradaan [8] used finite element analysis to assess the advantages of using a four-point bending fatigue test to localize where a crack could take place and how it developed in the specimen, obtaining very good numerical results that were validated posteriorly by experimental analysis.

In short, a fatigue failure is a very dangerous damage that could bring several problems since detection difficulties to complete component or total destruction. Therefore, the best way to prevent is to resort to full-scale structure analysis searching evidences of possible damages or address to NDI, for being a method with best advantages such as low cost or less inspection time.

2.3 Fracture Mechanics

Fracture mechanics is a field of material mechanical analysis, which includes general material behaviour during crack propagation and fracture. This discipline is very important to several engineering areas, such as aeronautical, space, naval and civil, with the aim to understand the causes and consequences of the material crack growth, and accordingly to the obtained results, provide solutions to the problematic situations, whilst always having in mind the structural integrity.
In the aeronautical field, fatigue is the major problem that brings fracture mechanics to act. Fatigue strength is by definition 'the maximum stress that can be repeated for a specified number of cycles without producing failure of the structural unit' [32], yet sometimes flaws arise in the material, that due to fatigue evolve into a crack, and posteriorly, to a fracture, that could compromise the integrity of the component, if not detected and repaired in time.
Starting with a concise differentiation of crack growth and fracture, where the crack growth is a slow process that occurs in a normal loading event - useful service life, as stated by Broek, D. [6], whilst fracture is a final action, with rapid development, that results in breaking the material in two parts, as can be seen in Figure 2.4.

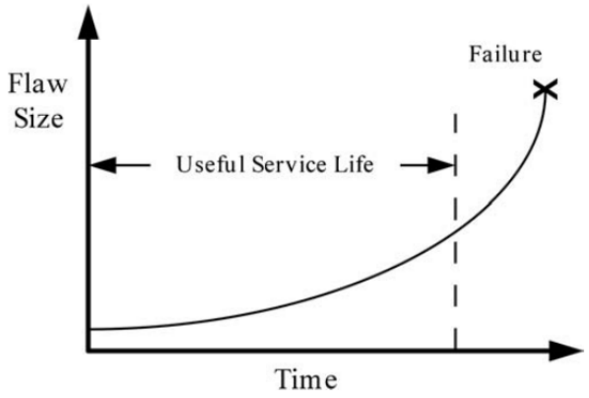

Figure 2.4: Flaw size in fuction of time [4].

Crack growth can appear due to several mechanisms, however the most frequent are due to [6]:

- Stress corrosion,
- Fatigue.

Both mechanisms can emerge isolated or aggregated. The first occurs due to sustained loading and the second appears due to cyclic loading and it will be approached in more detail.
A fracture can be a result of a crack, and it can only occur by two processes [6]:

- Cleavage - The material grains are, successively, splintered apart;
- Ductile rupture - Some aleatory particles (generally from alloy elements) break near the crack-tip creating some blank spaces that evolving to a fracture.

So, 'the fracture may be a consequence of a fatigue crack or a stress corrosion crack, but it occurs by cleavage or rupture' [6].

To understand fatigue failure, several models have been studied. The most adopted models are based in stress-life, the Miner's Rule, in strain-life, the Neuber's Rule and based in fracture mechanics, the Paris law.

Miner's rule is based on 'the damage caused by a cycle in a variable amplitude sequence is equal to that of a cycle of the same size under constant amplitude loading' [36], this means that every stress repetition has the same contribution, thus the first stress cycle contributes to damage as much as the last, and the component failure occurs when the damage sum reaches unity [36]:

$$\sum_{i=i} \frac{n_i}{N_{fi}} = 1 \quad (2.1)$$

Where n represent the number of cycles and N the theoretical number of cycles to failure.

In an elastic deformation, in a tip of a notch[1], the stress and strain factors assume an equal value. The same does not happen if the deformation has a plastic behaviour. Therefore, in a strain-life perspective, the Neuber's rule states 'under conditions of plastic deformation, the theoretical elastic stress concentration factor (K_t) is given approximately by the geometrical mean of the stress and strain concentration factors, (K_σ) and K_ε, respectively' [37], and it can be written as:

$$K_t = \sqrt{K_\sigma K_\varepsilon} \quad (2.2)$$

By a mechanic fracture perspective, the Paris law is described 'by the relationship between cyclic crack growth rate $\frac{\partial a}{\partial N}$ and stress intensity-range ΔK' [5].

$$\frac{\partial a}{\partial N} = C(\Delta K)^m \quad (2.3)$$

where C is a constant of the material, m is the slope on the log-log plot and $\Delta K = K_{[max]} - K_{[min]}$, which K_{max} represents the maximum and K_{min} the minimum values of stress intensity factor during a fatigue stress cycle.

The Paris law generates a typical kind of plot as it can be seen in Figure 2.5. It can be divided in three regions: crack nucleation, crack growth and final failure [33], and it needs an initial crack and constant stress range. In the crack nucleation region, the fatigue crack grows at a slow pace, and appears to approach a vertical asymptote at K_{th} - fatigue crack growth threshold, the minimum value of ΔK, which is interpreted as an absence of crack growth [5]. In the second region, exists a linear relation between the crack growth and the number of cycles, and it has a stable macroscopic crack growth, which predicts elastic behaviour [33]. At high growth rates, arriving at plastic phase, the curve become steep and it happens due to the small plastic zone [5], reaching the last region, where, eventually, fracture occurs. In that moment, the stress intensity factor acquires its maximum value - the fracture toughness (K_c) [33].

[1]The notch is an induced defect and crack is damage that could appear spontaneously or by notch evolution.

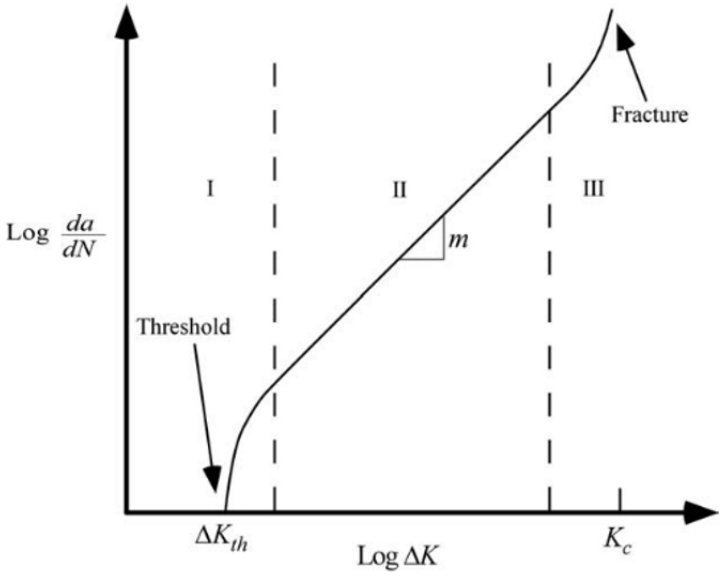

Figure 2.5: Paris Law plot for metals [4].

Habib, S. *et al* [33] applied this concept in the aeronautical field. An aircraft is subjected to a range of loading directly related to the flight phases and flight environment. For Paris Law to be applicable during the aircraft life, constant amplitude loading should be needed. It is based on its maximum and minimum stress level, that should be, respectively, take-off and rest [33].

2.3.1 Linear Elastic Fracture Mechanics - LEFM

One of the first attempt to try to explain the fracture behaviour was given by linear elastic fracture mechanics. Starting by an atomic view, the fracture is defined by its cohesive strength. This strength is responsible for keeping a specific atomic organization, and if some kind of external force is higher than cohesive strength, the atomic organization is disrupted, creating a flaw and a new atomic system. One consequence that can detect a flaw presence is the dropping of the global strength by magnifying the stress locally [4].

Fracture in atomic level works by the atomic organization disruption principle: some type of perturbation such as mechanical, thermal or chemical effect originates a rupture of atomic bonds. If the perturbation continues or increases during time, more and more atomic bonds will be broken, and this explains the atomic propagation of a crack, that can result in fracture.

Studied by Inglis[4], the first witness of stress concentration present in a flaw was originated by the study of elliptical holes in flat plates, equivalent to the Figure 2.6.

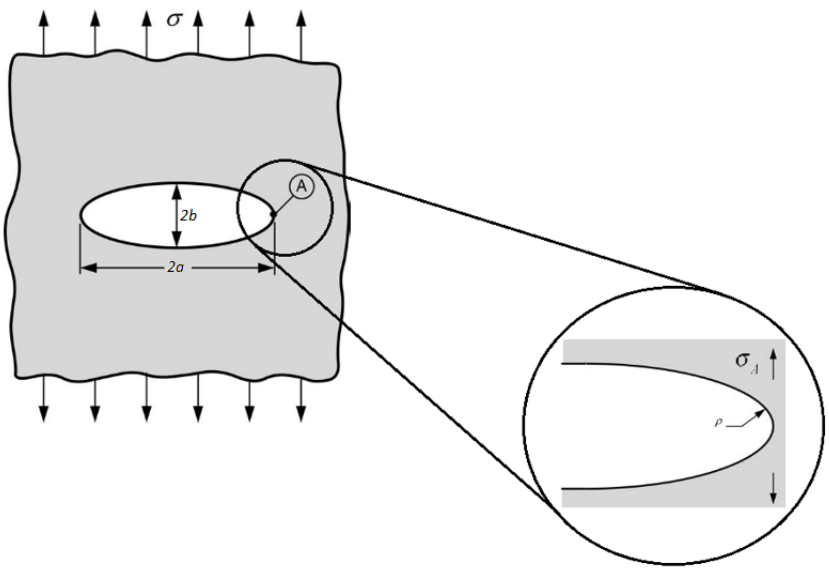

Figure 2.6: Schematic representation of elliptical holes in flat plates [4].

As can be seen, the elliptical hole has dimensions *2a x 2b* (width x height) and the plate is subjected to a width perpendicular stress σ - nominal stress[2]. Inglis assumed that the hole was not influenced by the plate boundary, that is, the plate width and height is much greater than *2a* and *2b*, respectively [4].
The stress near the hole is altered. Based on Figure 2.7 it can be noticed that far from the hole the stress is equal to σ, yet approaching the neighbourhood of the hole, along the x-axis, the value of σ_y has its maximum value at the tip of the hole [5].

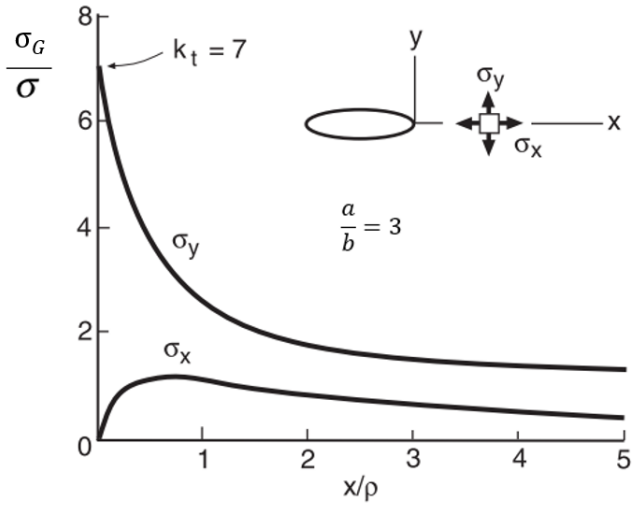

Figure 2.7: Particular case of stress distribution in an elliptical hole with $\frac{a}{b} = 3$, where σ_G represents general stress [5].

[2]The nominal stress can have different uses: it can be used as seen in Figure 2.6, as the uniform stress away form the notch, or sometimes it can be defined as the average stress in the section through the notch [6]. In this dissertation, the nominal stress will be approached as the first option.

Point A represents the crack-tip, and the stress concentration is given by:

$$\sigma_A = \sigma\left(1 + \frac{2a}{b}\right) \quad (2.4)$$

The ratio $\frac{\sigma_A}{\sigma}$ is defined as the stress concentration factor k_t:

$$k_t = \frac{\sigma_A}{\sigma} = \left(1 + \frac{2a}{b}\right) \quad (2.5)$$

When the hole is circular, $a = b$:

$$k_t = 3.0$$

Noted that in Figure 2.7, σ_A is displayed as σ_y and is directionally parallel to σ.
As the width hole increases comparatively to the height, the hole becomes sharper. In this case, Inglis changed the equation to:

$$\sigma_A = \sigma\left(1 + 2\sqrt{\frac{a}{\rho}}\right) \quad (2.6)$$

where ρ represents the radius of tip curvature:

$$\rho = \frac{b^2}{a} \quad (2.7)$$

When the hole width is immense relatively to the height, the equation above becomes:

$$\sigma_A = 2\sigma\sqrt{\frac{a}{\rho}} \quad (2.8)$$

The sharper the hole becomes, the more severe the stress concentration becomes, this means, theoretically, if b tends to zero, ρ also tends to zero, and with that σ_A tends to infinity [5].
In linear elastic fracture mechanics, there are two alternatives of analysis:

- The energy criterion;
- The stress-intensity criterion.

The first alternative 'states that crack extension (i.e. fracture) occurs when the energy available for crack growth is sufficient to overcome the resistance of the material' [4]. A theory initiated by Griffith and concluded by Irwin, based on the energy release rate G is given by:

$$G = \frac{\pi\sigma^2 a}{E} \quad (2.9)$$

where E is Young's modulus, σ is the remotely applied stress, and a is the half-crack length. This energy release rate is defined 'as the rate of change in potential energy with the crack area for a linear elastic material' [4]. When the fracture occurs, $G = G_c$ and the energy release rate becomes a measure of fatigue toughness which means that G_c is the material's resistance to fracture.

$$G_c = \frac{\pi\sigma_f^2 a_c}{E} \quad (2.10)$$

Fatigue toughness, G_c, is body cracked independent, which means that it does not depend on its size or geometry, so this parameter should be applied to a structure. In this case, the material's

behaviour should be linear elastic. In the fracture moment, G is the driving force and G_c is a measure of material resistance.

A modification occurred to the previous equation, given by Irwin and Orowan. The modification allowed to create an equation that could be applied to materials with plastic flow [4]:

$$\sigma_f = \left(\frac{2E\omega_f}{\pi a}\right)^{\frac{1}{2}} \quad (2.11)$$

Where ω_f is the fracture energy that varies depending the material behaviour.

If the material has a plastic behaviour, as metals, $\omega_f = \gamma_p + \gamma_s$, and if it is an ideally brittle material, $\omega_f = \gamma_s$; where γ_p is the plastic work per unit area of surface created, γ_s reflects the total energy of broken atomic bonds in a unit area, in a brittle solid.

The stress-intensity criterion is defined by stress distribution that characterize an element near the tip of the crack in an elastic material, as can been seen in Figure 2.8. This criterion in each stress component represents a proportionality to a constant called stress-intensity factor, K, that characterizes the crack-tip conditions in a linear-elastic and isotropic material. This constant is a measure of the severity of a crack situation [5].

$$K = \sigma\sqrt{\pi a} \qquad (a << b) \quad (2.12)$$

When a fracture occurs, it means that occurred a local failure of the material due to some stress and strain forces, and so the fracture must occur at a critical stress intensity, K_c. In this case, $K = K_c$ and K_c represents the fracture toughness, a measure of material resistance that represents a 'measure of a given material's ability to resist fracture in the presence of a crack' [5], and it depends on temperature, loading rate and thickness properties.

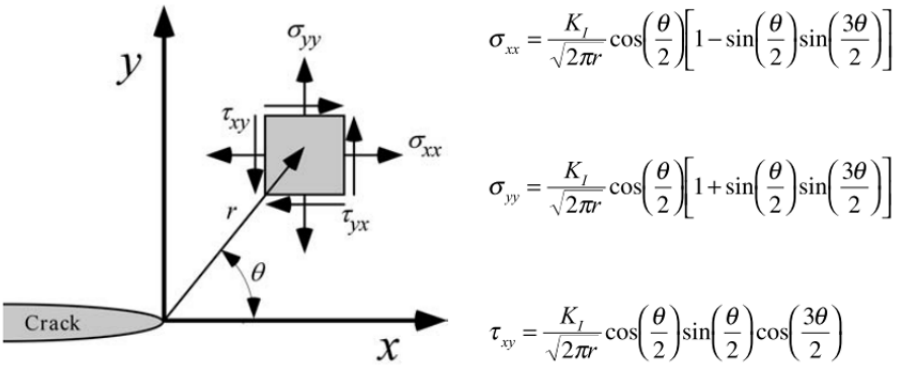

Figure 2.8: Representation of stresses near the tip of an elastic material (r and θ are polar coordinates) and respective equations to mode I loading [4].

At the moment of fracture, $K = K_c$ and $\sigma = \sigma_c$, which in this case represents the critical value of remote stress necessary to cause fracture, and using the equation (2.12):

$$\sigma_c = \frac{K_c}{\sqrt{\pi a}} \quad (2.13)$$

These two analysis of crack treatment, the energy criterion and the stress-intensity criterion,

can be correlated by equation (2.14)

$$G = \frac{K^2}{E} \quad (2.14)$$

There are three types of behavior that a cracked body can experience accordingly to its loading. Mode I loading is denominated as opening mode [5] where the tension load is applied normal to the crack plane [4] with the faces of the crack separating along the body. Mode II loading, called sliding mode, is caused by in-plane shear loading, and one of the face crack tends to slide to the other one [4]. And, finally, mode III, denominated as tearing mode, is also caused by shearing loads, but applied out-of-plane [5].

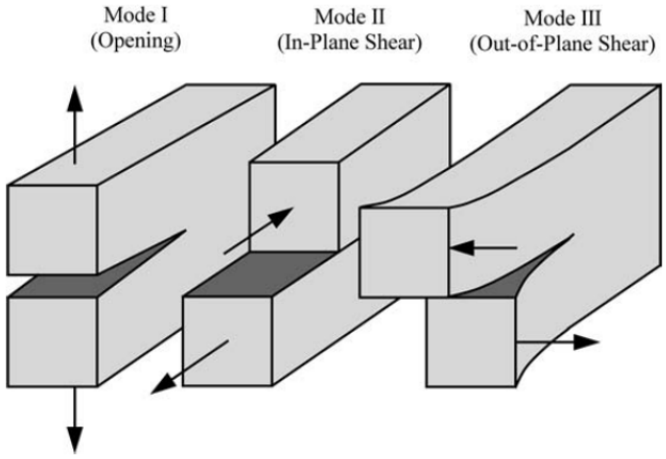

Figure 2.9: The different modes of loading [4].

A crack can result of a combination of these modes individually or a combination of them.

The Equation (2.12) depends on geometry and mode configuration. So, a general equation can be written:

$$K_{(I,II,III)} = Y\sigma\sqrt{\pi a} \quad (2.15)$$

where Y is a dimensionless constant that depends on the geometry and the mode of loading.

To sum up, the linear-elastic fracture mechanics is a very important tool. Although having an analyis only on brittle materials or materials with a small plastic behaviour, this approach can reach innumerous material types and characterizes many behaviours. Figure 2.10 represents a diagram of failure stress versus fracture toughness K_c and it can be detected that in a lower K_c the fracture is conducted as brittle fracture, this means, by LEFM concepts. Alongside the increase of K_c, the fatigue failure arrives to nonlinear fracture mechanics, that try to explain the gap between LEFM and bankruptcy [4]. Arriving to high K_c, LEFM is not valid and 'failure is governed by the flow properties of the material' [4].

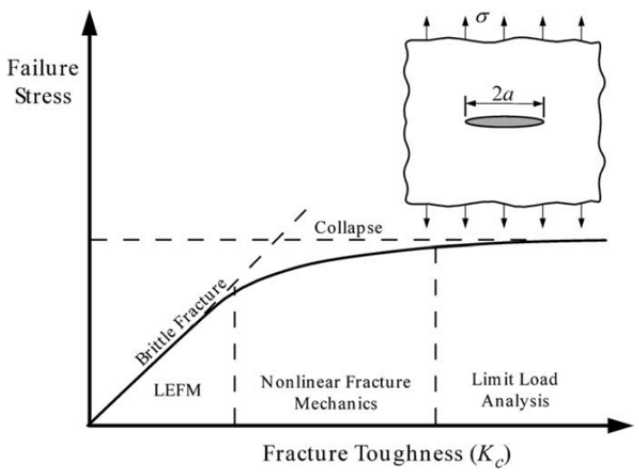

Figure 2.10: Relation between Fracture Toughness K_c and Failure Stress in evolution of crack propagation [4].

2.3.2 Elastic-Plastic Fracture Mechanics - EPFM

Previously, in Section 2.3.1, it was demonstrated how LEFM has a huge impact to explain the fracture along an infinite plate subjected to infinite stress. Also, it was concluded that LEFM was not enough to explain all fracture behaviour in all kind of materials. There were some restrictions that LEFM could not explain the fracture comportment, as 'inelastic material deformation, such as plasticity in metals and crazing in polymers' [4].

In some materials, with small plastic zone, the LEFM can still be applicable, and it is called the region of K-dominance (or K-field). If K-dominance is eliminated, the K stops to characterize the crack behaviour. When this event occurs, other approaches have to be created to respond to the remaining questions to materials with time-independent and non linear behaviour.

Appealing only to metals, when a crack develops, in the crack-tip proximity, plastic deformation can occur (region of yielding) and it is called plastic zone.

For the understanding of the bridge between brittle and ductile materials:

$$a_t = \frac{1}{\pi}\left(\frac{K_c}{\sigma_0}\right)^2 \quad (2.16)$$

when a_t is greater, the strength will be limited by brittle fracture. On the other hand, if a_t is lower, the dominant behaviour will be yielding.

These materials, with plastic deformation, were the cause for the develop of two principals approaches:

1. The $J - integral$
   This method is capable of managing large bulk of yielding, and it is 'equal to the energy release rate in a nonlinear elastic body that contains a crack' [4].

   This definition is analogue to the energy release rate for linear materials - G, but in nonlinear materials, the G parameter is substituted by J.

   As J characterizes the crack-tip behaviour in a non-linear elastic material, a power law was given, called the Ramberg-Osgood equation [4]:

   $$\varepsilon = \frac{\sigma}{E} + \alpha\frac{\sigma_0}{E}\left(\frac{\sigma}{\sigma_0}\right)^n \quad (2.17)$$

   Here, exists a relationship between strain and stress, included elastic strain and where:
   σ_0 – Yield strength
   ε – Strain
   E – Young's modulus
   α – Material dimensionless constant
   n – Strain-hardening exponent

   For materials with elasto-plastic behaviour, J is only significant in measure the intensity of stress and strain parameters in the vicinity of the crack-tip, however it loses the potential energy interpretation [5].

2. CTDO (Crack-Tip Opening Displacement) - δ
   This approach estimates the displacements in the separation of the crack faces near the tip, as can be seen in Figure 2.11.

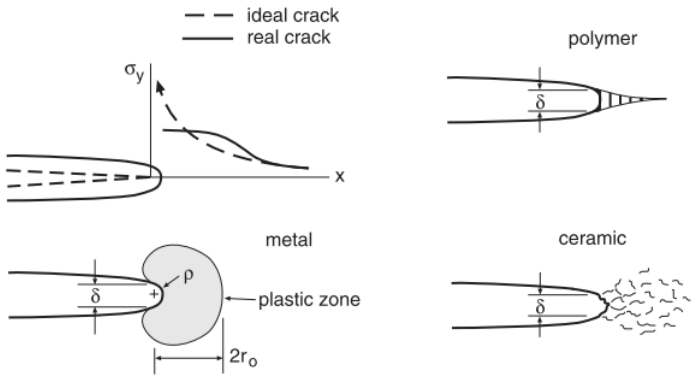

Figure 2.11: Various crack types in different materials, producing plasticity, crazing or micro cracking [5].

As showed for different materials, the crack-tip behaviour changes and the stress is no longer infinite, so the crack is open by δ.

For ductile materials, the equation that defines δ is given by:

$$\delta \approx \frac{K^2}{E\sigma_0} \approx \frac{J}{\sigma_0} \quad (2.18)$$

Both are tools to understand and characterize crack growth in most of real materials, and they can be used for engineering purposes when used with full concepts' understanding and acknowledge.

2.3.3 Plane stress versus plane strain

Making a brief definition of plane stress and plane strain with respect to the crack-tip and starting with plane stress that is applicable to thin solids. Having in mind the Figure 2.8 it can be noticed that in the crack-tip the stress are biaxial. In the face of the crack-tip (plane XY), is presented a free surface, which is a case of plane stress:

$$\sigma_z = 0 \quad (2.19)$$

and consequently, there does not exist a shear stress, yet exists strain:

$$\begin{aligned} &\tau_{zx} = \tau_{xz} = 0 \\ &\tau_{zy} = \tau_{yz} = 0 \\ &\varepsilon_z = -\nu\frac{\sigma_x}{E} - \nu\frac{\sigma_y}{E} \neq 0 \end{aligned} \quad (2.20)$$

So, for fracture analysis, as the thickness is smaller compared to the plastic zone, the Poisson effect[3] occurs in the crack-tip, and the yielding on shear inclined planes starts to exist. The fracture tends to follow the development along these inclined planes, resulting in inclined fractures [5], as can be seen in Figure 2.12b.

[3]The Poisson effect results of a phenomenon of material expansion in the perpendicular directions from where the compression direction was applied.

The plane strain, on the other hand, is applicable to thick solids. Moving away in the thickness directon of the crack-tip, it can be found a triaxial state of stress [6] completely constrained, where the stain perpendicular to the plane is non-existent:

$$\varepsilon_z = \frac{\sigma_z}{E} - \nu\frac{\sigma_x}{E} - \nu\frac{\sigma_y}{E} = 0 \quad (2.21)$$

and consequently, there does not exist angular deformation in that direction:

$$\begin{aligned} \gamma_{xz} = \gamma_{zx} = 0 \\ \gamma_{yz} = \gamma_{zy} = 0 \end{aligned} \quad (2.22)$$

However, it still has stress in z-direction:

$$\sigma_z = \nu(\sigma_x + \sigma_y) \quad (2.23)$$

In this situation, occurs a flat fracture through over most the thickness, and this happens due to an increase of the yielding on σ_y direction reducing the plastic zone size [5].

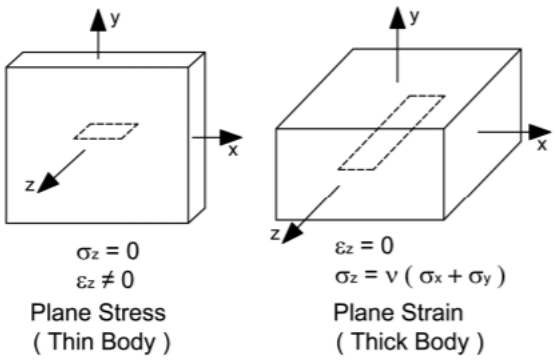

(a) Plane stress vs plane strain representation [38].

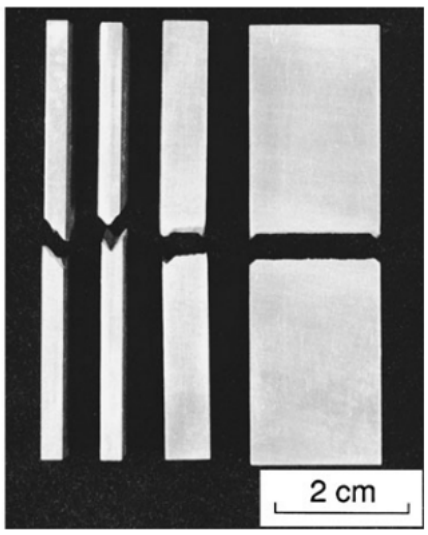

(b) The type of fracture in both cases [5].

Figure 2.12: Planes representation and the result on fracture.

The K_c is directly linked to the solid thickness, which means that, with the increasing of thickness, K_c tends to decrease, until it reaches a worst-case value, K_{Ic} - plane strain fracture toughness. If the material, relatively to the solid thickness, presents a small plastic zone surrounding the crack-tip, a state of plane strain is identified. In this case, the crack growth rate is low, giving to K and K_c similar values, and K becomes the standard plane strain fracture toughness for mode I, K_{Ic}, that represents the 'worst case of fracture toughness that can be used for any thickness' [5].
There exists a transitional flow starting with plane stress and finishing with plane strain, as can be seen in Figure 2.13. The plane strain can be identified with K_{Ic}, however it can be used the same notation or K_c for plane stress or transitional [6].

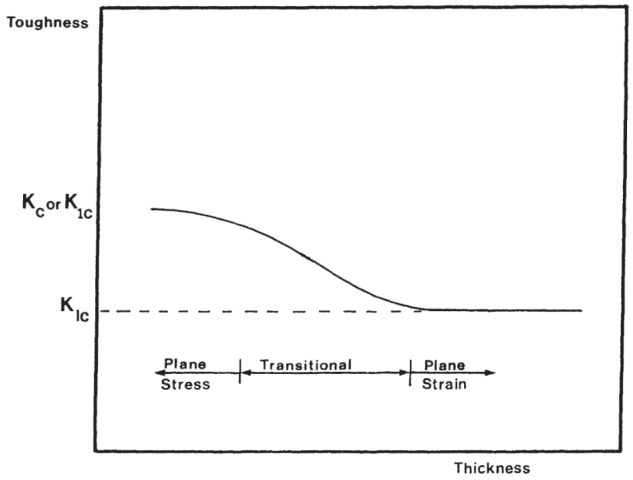

Figure 2.13: K_c between planes with the increase of thickness [6].

For some cases of cracks initial configuration, the plane is already defined. As seen in Figure 2.14 the surface flaws and corner cracks are defined as plane strain, in their majority localized in the center. So, independently of the thickness, for these configurations the K_{Ic} is used [6].

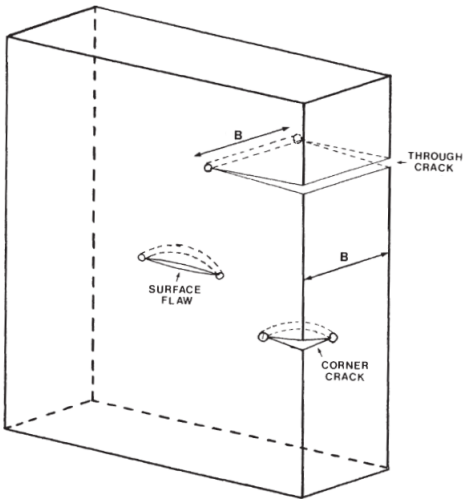

Figure 2.14: Representation of various crack configurations [6].

Chapter 3

Numerical Study

The purpose of this chapter is to provide the methodology and the theoretical concepts for fatigue testing. In this chapter the four-point bending loading conditions are presented. It is also presented the fatigue loading methodology for crack growth.
The principal equations of the four-point bending test are demonstrated for the present case of study. A crack description and a brief approach to the stress distribution for the specimen with the presence and absence of crack are made. This chapter is important to understand all the numerical configuration and its respective behaviour.

3.1 Methodology

The methodology presented is a fundamental step to link the theoretical concepts to the numerical configuration, and later on, the results.
This dissertation main objective is the use of numerical/analytical approaches to develop a new methodology to manufacture shallow fatigue cracks for the qualification of NDT technologies. A four point bending setup was selected to generate the loading conditions that will lead to a crack propagation through the specimen thickness when fatigue loaded. The specimen geometry selected was a MT (middle tension) specimen, since it is in agreement with major fatigue standards and it is easily adapted for four point bending testing, discussed in more detail in Chapter 4. To estimate the number of loading cycles that are needed for a crack starting at an initial notch to achieve a predefined length it is necessary to determine, using LEFM together with FEM (Finite Element Method), the values of the stress intensity factor, and then followed by an analytical approach, retrieve the number of fatigue cycles. In a posterior stage, supported by the software NASGRO®, a comparison between results of the fatigue cycles obtained are made. There are various methods to induce fatigue, such as: tension fatigue tests accomplished by Schubbe [39] that used pin-loaded compact tension specimens to mesure crack growth rates for different thickness. Molent *et al.* [40] subjected a dog-bone specimen to bending and compression fatigue stresses in order to determine the surface finishing texture and the application of load spectra influence to crack initiation. Guedes [41] stated that the main fatigue tests that could be performed to study damage evolution are tension-tension loading tests, where stress ratio R has an apparent effect on crack growth; tension-compression and compression-compression fatigue, where is observed that fatigue life is shorter when compared with tension-tension loading. Considering that the previous cases never achieve the bending conditions, these cases are demonstrated in bending fatigues tests, where several differences are evidenced, such as 'stresses, strains and damage distribution which varies along the gauge length of the specimen' [41] differently of what occurs in tension-compression tests. Some differences can be found in FEM implementation, where damage growth may be difficult to determine due to its diversity of values for each specimen point. However, for an experimental scenario it is easier to obtain results using bending fatigue tests, due to the fact that larger displacements can be obtained by applying smaller forces allowing a simpler design fatigue instrumentation. There

are three bending fatigue test methods: three-point bending, four-point bending and cantilever bending.
Four-point bending test method was chosen since the objective is to promote a constant bending moment that will impose a through the thickness preferential growth direction, without achieving fracture and restraining as much as possible the crack propagation along the surface. With all these constraints, the three-point bending fatigue test is not considered the best option. The configuration of this previous method is based on a single loading force applied on the crack plane direction, meaning that, the crack would be subjected to maximum stress, causing difficulties to restrain the crack propagation. Garcia C. et al. [42] used the four-point bending fatigue test in numerical and experimental setup where the residual stress fields of a fatigue crack growth were obtained. Baxter et al. [43] were capable of performing this method to study a fatigue crack growth in an aircraft landing gear where the crack propagation was detected using acoustic emission.
In summary, the methodology used in this dissertation is a MT pre-cracked specimen subjected to a four-point bending fatigue test, where the crack propagation is preferentially made along the specimen thickness.

3.2 Four-Point Bending Test Configuration

A four point bending fatigue test consists on an evaluation of the material behaviour under cyclic loading.
The configuration of this test is presented in Figure 3.1.

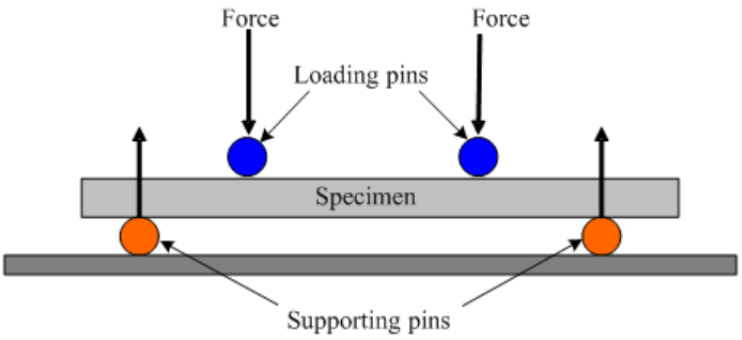

Figure 3.1: Configuration of four-point bending test [7].

It can be observed that the four-point bending test consists of two loading pins that are symmetrically set to one and a half or one and a third of the specimen length and two supporting pins. The specimen has a constant rectangular cross-section. According to ASTM (American Society for Testing and Materials) D6372 - Standard Test Method for Flexural Properties of Unreinforced and Reinforced Plastics and Electrical Insulating Materials by Four-Point Bending the loading and the supporting pins should have cylindrical surfaces and its radius shall be $5.0 \pm 0.1mm$. Regarding the positions of the two supporting pins, they shall be at least 10% from the edges of each end of the support span [44].
Figure 3.2 exposes the free body configuration for this dissertation case. Between the supporting pins, the specimen is divided by three equal parts, however from the specimen edges to the supporting pins, the distance is equal to one and tenth of the specimen length. The shear and

bending moment diagrams are also presented.

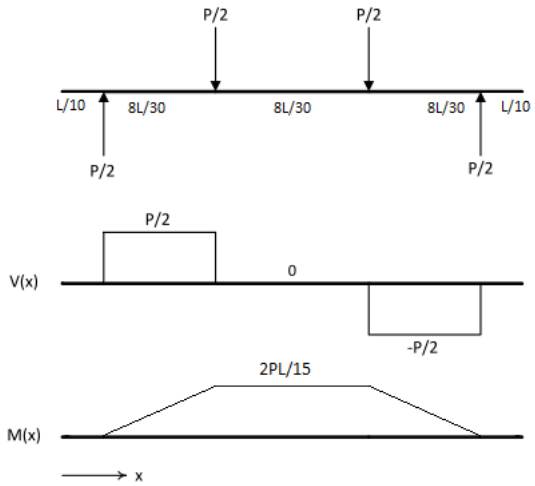

Figure 3.2: Free-body and respectively shear $V(x)$ and bending moment $M(x)$ diagrams [8].

In this case, P represents the total applied load and L the beam total length. It can be noticed that between the inner supports, the shear load is null and the bending moment reaches its maximum and maintains its value, given by $M = \frac{2PL}{15}$.

The bending stress can be calculated by:

$$\sigma = \frac{Me}{I} \quad (3.1)$$

where M is the bending moment, e the vertical distance from neutral axis to edge and I is the area moment of inertia about the bending axis [8], [5], given by: $I = \frac{t^3 W}{12}$, where W is the width component and t the thickness. Adding this information to Equation (3.1):

$$\sigma = \frac{4PL}{5t^2 W} \quad (3.2)$$

This method of fatigue testing allows the study of 'fatigue properties of interest, while simultaneously retaining the prevailing in-service surface condition of the material from which the specimen is extracted, as well as being able to fluctuate the stress on the specimen surface fully between tension and compression' [8].

Fatigue stress is characterized by cyclic loading that can have constant amplitude, as for example in fatigue tests. The stress ratio R describes the stress fluctuation, which is defined as the ratio between minimum and maximum force in one cycle [8], and has a great influence on the fatigue life [35].

$$R = \frac{P_{min}}{P_{max}} \quad (3.3)$$

The results of the four-point bending fatigue test can be obtained by a fatigue stress curve of a material, $S-N$ graph. A typical $S-N$ curve is described in Figure 3.3a, and a comparison with the strain-stress curve is presented, Figure 3.3b, which results from the material mechanical properties.

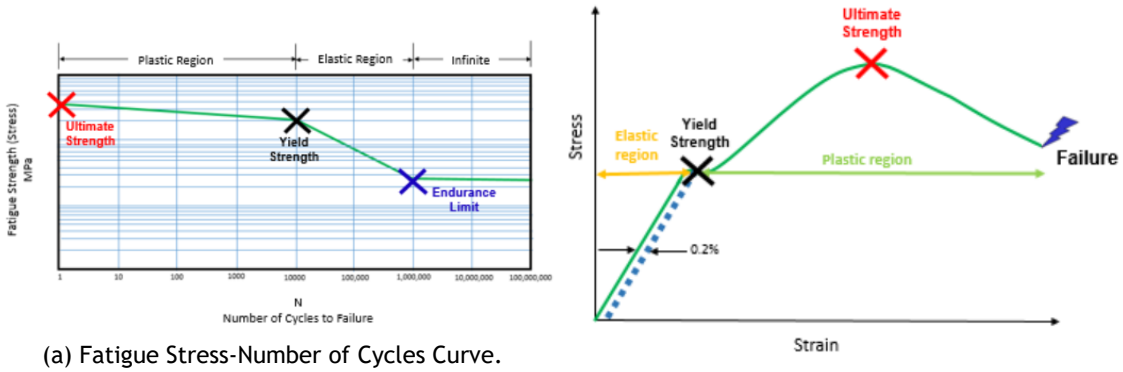

(a) Fatigue Stress-Number of Cycles Curve.

(b) Stress-Strain Curve.

Figure 3.3: A comparison between graphs that provide material mechanical properties [8].

There exists a correlation between $S - N$: the number of cycles until fracture increases as the stress range decreases. At a certain point, this correlation is no longer visible, and even though it has an increase in the number of cycles, the stress range stays constant. For this situation, an infinite number of cycles can be applied in the material without it achieving fracture - fatigue limit of the material - S_f [8].

3.3 Crack Initiation and Stress Distribution

When the four-point bending test is executed, the upper surface, where the loading pins are located, is subjected to compression loading whilst the lower surface is subjected to tension loading. As a result of these loading variations and the tensile stress having a greater impact, the corresponding crack shall appear in the lower surface in consequence to a failure [9], which is represented as critical area in Figure 3.4. As the initial damage will be introduced at the middle span (between the loading pins in the xz plane), the crack shall propagate through this section, being its maximal propagation in depth (negative y direction) and having a small progression in length into the surface.

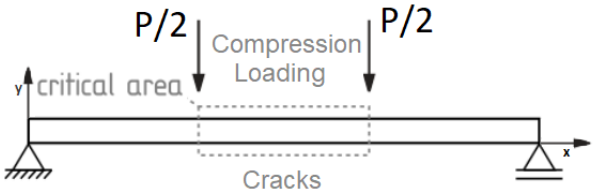

Figure 3.4: Loading variation in the four-point bending test (Adapted from [9]).

As the maximum bending moment is reached between the two loading pins, which is characterized by pure bending, the results obtained are a linear stress distribution over the cross section, which is a rectangular section, as can be seen in Figure 3.5. While the crack is not induced, the cross-section stress distribution is represented as in Figure 3.5, on the left side. Generally, the neutral axis, at this stage, is stress-free. Nonetheless, when the crack is induced, the neutral axis suffer a shift in the opposite direction of the crack and the former neutral axis is exposed to stress and, therefore, to strain [9], as can be seen in Figure 3.5 on the right side.

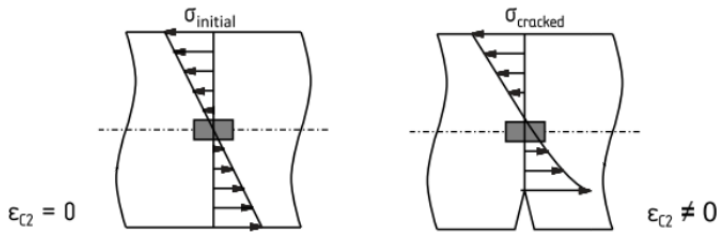

Figure 3.5: Cross-section stress distribution: without crack (left) and with crack (right)[9].

Chapter 4

Numerical Results and Discussion

In this chapter the numerical and analytical approach will be described, as well as the results and respective discussion. The model and results were developed with the support of FEM Abaqus® software and NASGRO®.

This chapter is divided in three main sections. In the first section, the material properties of the specimen are given, as well as, its geometric dimensions.

A general numerical modelling is described for both softwares, which are separated by subsections. In the first subsection is described the FEM Abaqus® software where the loading and boundary conditions are described, the crack interaction, the pseudo-code and a mesh analysis is also presented to have a numerical validation of the results. The second subsection is dedicated to NASGRO® numerical modelling with a description of the initial conditions, the governing equations and the respective pseudo-code.

The Abaqus® and NASGRO® results and its discussion are presented in the third section. In the Abaqus® subsection a mathematical remark is made to complement the results.

4.1 Material

The considered specimen is a MT type with the dimensions of $280mm$ x $100mm$ x $2mm$ (length x width x thickness). The initial notch geometry has a rectangular shape, for simplification purposes, located in the middle of the specimen. The notch was dimensioned as $4mm$ for length size, which is denoted as $2c$, and a depth size denoted as a, that will be calculated in Section 4.3.

According to ASTM E-647 - Standard Test Method for Measurement of Fatigue Crack Growth Rates[45], for the notch root radius ρ inferior to $0.25mm$, the notch preparation should be induced by electrical discharge machining.

The notch root radius for this case is supposed to be near zero for being a sallow crack (see Section 2.3.1, Equation (2.7)):

$$\rho = \frac{b^2}{a} = \frac{0.01^2}{2} = 5 \cdot 10^{-6} mm$$

For better theoretical coherency, the notch geometry should be semi-ellipsoidal.

The material used in this numerical experiment was AA7050-T7451 aluminum alloy.

The 7050 Aluminum alloy is used in numerous aviation components, such as bulkheads, spars, skins, frames, stringers, ribs, brackets of aircraft landing gears and other bearing components [46]. This type of alloy is used in commercial and military aircraft due to its high resistance to corrosion, high fracture toughness and a very good fatigue resistance.

The material element properties are described in Table 4.1.

Table 4.1: Material Element Properties of AA7050-T7451 Aluminum Alloy [11]

Elements	Aluminum	Zinc	Copper	Magnesium	Zirconium
%	87.3 - 90.3	5.7 - 6.7	2.0 - 2.6	1.9 - 2.6	0.08 - 0.15
Elements	Iron	Silicon	Manganese	Titanium	Chromium
%	<= 0.15	<= 0.12	<= 0.10	<= 0.06	<= 0.04

NASGRO® is recognized beyond its fracture behaviour features, although having a considerable stress intensity factor library of an extensive list of geometries with crack growth parameters, the software has, as well, material mechanic properties for different environments and crack orientations.
The material properties of aluminum alloy AA7050-T7451 are given by NASGRO® library and they are thickness dependent. Therefore, since a plate thickness of $2mm$ is not available in the library, the properties of a thickness of $9.6mm$ $(3/8in)$, which the closes to the specimen thickness, were adopted.
The heat-treatment of this alloy makes it an anisotropic material and its strength properties are well defined. However, data available for L-S[1] orientation are insufficient, having more available data for L-T, T-L, and S-L orientations [47]. To apply the LEFM concepts the material was considered isotropic for simplification purposes.
The material mechanical properties, shown in Table 4.2, were obtained through NASGRO® (Ultimate and Yield Tensile Strength) and MatWeb [11].
The material has L-T orientation and it was built at dry humidity air as specific atmospheric environment.

Table 4.2: Mechanical Properties of 7050-T7451 Aluminum Alloy [11]

Mechanical Property	
Ultimate Tensile Strength	$537.8MPa$
Yield Tensile Strength	$468.8MPa$
Poisson's Ratio	0.33
Modulus of Elasticity	$71.7GPa$
Fracture Toughness (L-T)	$1113.1MPa\sqrt{mm}$

4.2 General Procedure

This section is divided in two main parts: Abaqus® Numerical Modelling and NASGRO® Numerical Modelling, where the procedure implemented in each stage is explained in detail as well as the numerical configuration in both softwares. There was a necessity to create this section for better clarification and organization of this dissertation since several attempts were made to obtain viable results.

4.2.1 Abaqus® Numerical Modelling

Abaqus® is a software of finite element analysis developed by Hibbitt, Karlsson $\&$ Sorensen, Inc. in 1979, which posteriorly has been acquired by Dassault Systèmes with its first version launched in 2005.
To analyse the problem, Abaqus® software version 2018 was used with a specific interaction on the crack domain - Contour Integral.

[1] In section 4.1, S represents long transverse direction and L represents rolling direction

4.2.1.1 Numerical Validation

A comparison was performed to accomplish the numerical validation between the numerical and the analytical perspective, presented in Section 3.2.

The main objective of this section is to demonstrate the load value that should be applied to the load pins. Having the maximum stress defined as $\sigma = 430MPa$ between the supporting pins, and considering the equations in Section 3.2, the load value was determined as $P = 767.86N$. The stress value was defined as $\sigma = 430MPa$, due to its proximity to the material's yield tensile strength, and therefore assess the specimen behaviour in a critical situation.

A mesh convergence study was performed to validate the numerical results. The linear brick type elements with reduced integration ($C3D8R$) were chosen due to its low computation time whilst providing the same accuracy given by $C3D8$ elements. Furthermore, zones of interest were locally refined in a cubic region.

The FEM is dependent on the mesh size and geometry attribution, so a mesh convergence to maximum principal stress was made in a specific critical node to ensure that the results would be as accurate as possible. The values are presented in Table 4.3 and the number of elements are only associated to the specimen.

Table 4.3: Mesh Convergence Study

Number of Elements	Maximum Principal Stress [MPa]	Error [%]
16224	379.76	11.7
18048	380.08	11.6
19776	377.66	12.2
24336	404.74	5.9
27072	406.33	5.5
29664	401.61	6.6
40560	443.69	3.2
45120	445.91	3.7
49440	430.83	0.2
55160	425.20	1.1
76880	422.07	1.8
83280	421.90	1.9

The results obtained by the mesh convergence study are plotted for better interpretation. In Figure 4.1 the mesh convergence for the maximum principal stress is presented and in Figure 4.2 is shown the error convergence related to the value of $\sigma = 430MPa$.

According to the aforementioned information, it can be concluded that the convergence is achieved. The mesh chosen can be seen in Figure 4.3, with a total of 97360 elements: 83280 elements in the specimen and 14080 elements in the four pins.

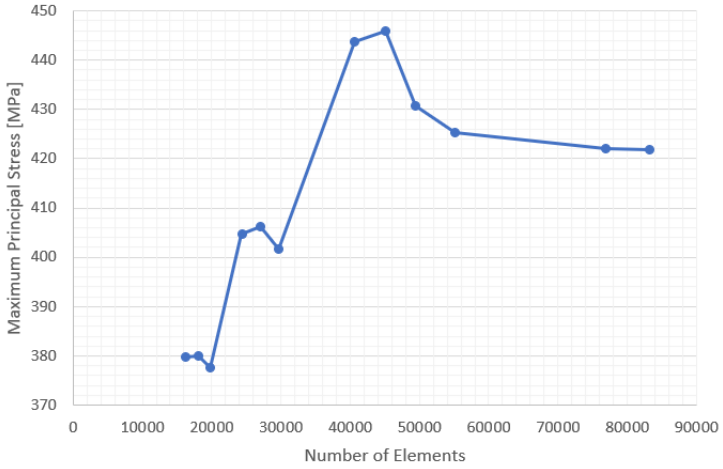

Figure 4.1: Convergence of the Maximum Principal Stress.

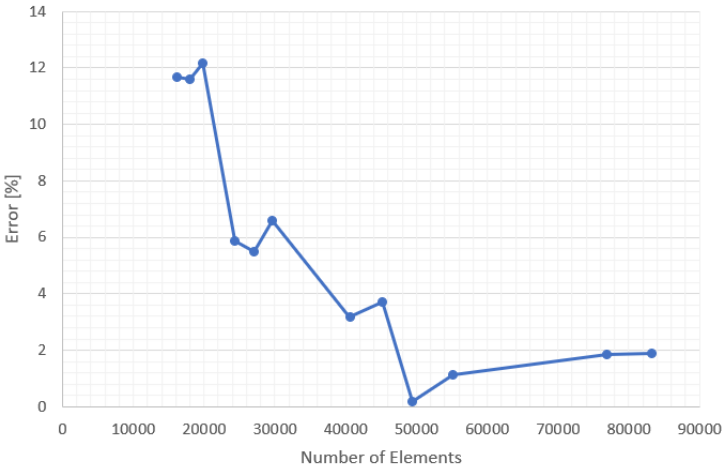

Figure 4.2: Error convergence for the value of $\sigma = 430MPa$.

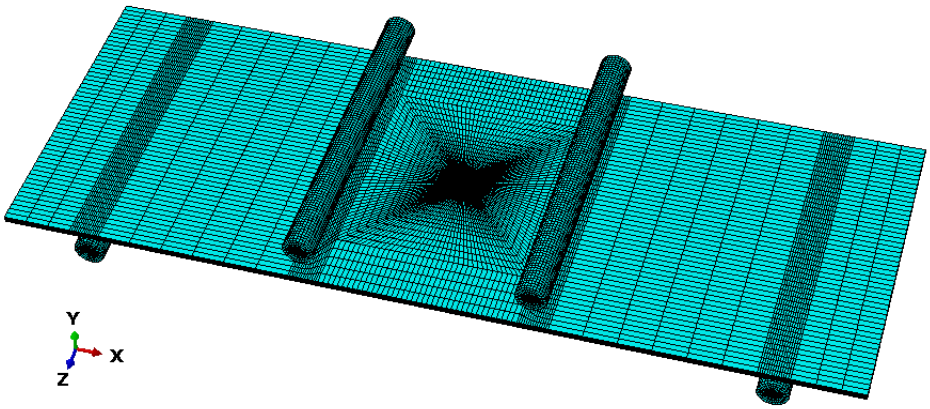

(a) General Mesh assignment.

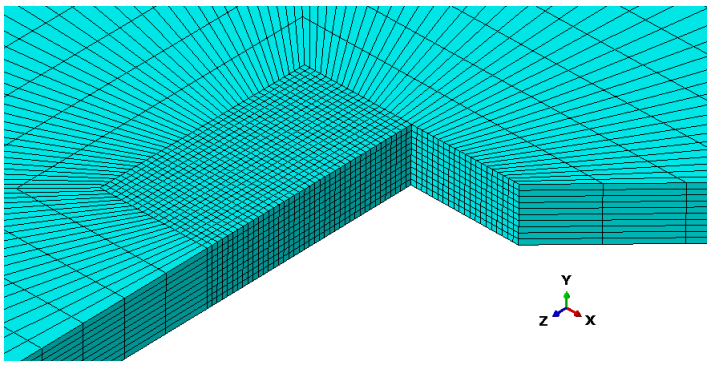

(b) Local mesh configuration for crack zone.

Figure 4.3: Mesh configuration given to the considered model.

The difference between analytical and numerical validations can be seen in Figure 4.4. A small difference can be noticed in the critical area, between the loading pins, where the stress value should be equal to $430MPa$. A maximum difference of 9.19% was verified.

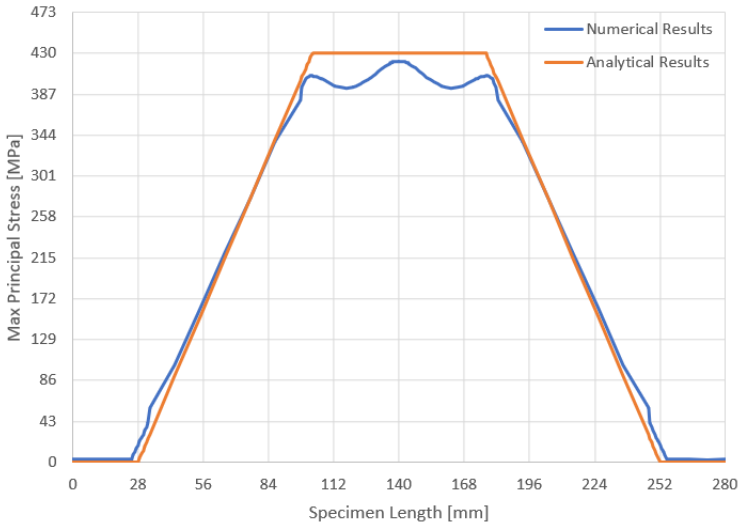

Figure 4.4: Comparison between the numerical and analytical results relative to the maximum principal stress along the specimen length.

After numerical validation, it became realistic to proceed to the crack characterization.

4.2.1.2 Boundary conditions

A 3D-solid deformable pre-cracked specimen and four pins modeled as rigid bodies were designed. After applying the material properties to the specimen, the boundary and loading conditions were defined.

The simulation was made in four steps: the initial step was defined by default in Abaqus® to set up possible initial conditions [42], the second step that allowed the positioning of the loading pins and the specimen, a third step to ensure the contacts between the pins and the specimen and the last step to apply the load.

A fixed condition was applied to the supporting pins, and a vertical free-displacement with a vertical loading was imposed on the loading pins. A restriction in the middle of the specimen was also imposed to restrain its movement.

The initial crack was represented as a rectangular format, for simplification purposes, with the dimensions observed in Table 4.4.

4.2.1.3 Crack

As one of the main goals of this dissertation was to determine the stress intensity factor along the crack depth, the Contour Integral method was used for this accomplishment.

The crack front, the crack tip, and the crack extension direction were defined to assure a crack propagation through thickness until the crack limit imposed is achieved.

4.2.1.4 Abaqus® Pseudo-code

An Abaqus® pseudo-code is presented in this section. The pseudo-code is an important tool to understand the basic software operations as well as to identify the governing equations. Here, the mesh elements receive the main focus, where a *while* function is used in the load step to explain how the software operates in every stage of the loading application.

Algorithm 1 Abaqus® Pseudo-code

procedure START($Abaqus$)
    Step1 = Set initial parameters (geometry, material, notch)
    Step2 = Set the right positions of specimen and the four pins
    Step3 = Set contacts between the specimen and the pins
    Step4 = Set load in the loading pins
        $mesh\_elem = 0$
        $vector\_mesh\_elem = 0$
        while $mesh\_elem \leq 97360$ **do**
            Calculate the maximum principal stress for the four Point Bending test

$$\sigma = \frac{4PL}{5t^2W}$$

▷ Equation (3.2)

            Calculate the stress intensity factor in the crack region

$$K_{(I)} = Y\sigma\sqrt{\pi a}$$

▷ Equation (2.15)

        Update solution along $vector\_mesh\_elem$
        $mesh\_elem = mesh\_elem + 1$
    Print results

4.2.2 NASGRO® Numerical Modelling

Initially developed by NASA (National Aeronautics and Space Administration), in 1980, NASGRO® is a software code that performs fracture control analysis. An analysis of different types of fatigue and fracture mechanics are possible due to its different programs.

This software allows choosing the crack and specimen geometry, so it was selected the option SC30 - Semi-elliptical surface crack (offset) in plate, as can be seen in Figure 4.5 with the required initial conditions, presented in Table 4.4.

This geometry was the best choice for this study case where a rectangular specimen is represented and the notch is totally defined in the specimen. Regarding to the others parameters, $S1$ is the bending stress in the thickness, which means, it is the stress perpendicular to crack plane; $S0$ represents the tension or compression stress and it is absent in this study case.

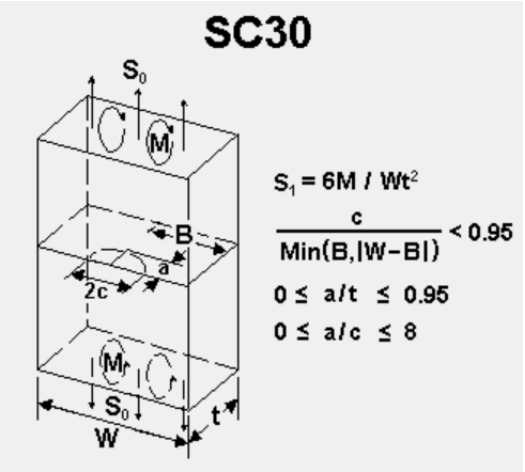

Figure 4.5: Crack case given by NASGRO®.

Regarding the crack growth model, a non-interaction model with NASGRO equation constants was used. According to Mettu *et al* [48], NASGRO equation is given by:

$$\frac{\partial a}{\partial N} = C\left(\Delta K_{eff}\right)^{m} \frac{\left(1 - \frac{\Delta K_{th}}{\Delta K}\right)^{p}}{\left(1 - \frac{K_{max}}{K_c}\right)^{q}} \quad (4.1)$$

where N represents the number of applied fatigue cycles and a represents the half crack length. ΔK, ΔK_{th} and ΔK_{eff} are the stress intensity factor range, the threshold stress intensity factor and the effective stress intensity factor, respectively. The maximum stress intensity factor and the critical stress intensity factor are represented as K_{max} and K_c. C, m, p, q are material constants[2].

The ΔK_{eff} can be expressed as a function of ΔK and U in the form:

$$\Delta K_{eff} = U \Delta K \quad (4.2)$$

where U is given as a function of stress ratio R, which was defined as $R = 0.1$, and Newman's crack opening f[3]:

$$U = \frac{1 - f}{1 - R} \quad (4.3)$$

The Newman's crack opening f is described as:

$$f = \frac{K_{op}}{K_{max}} = \begin{cases} max(R, A_0 + A_1 R + A_2 R^2 + A_3 R^3), & R \geq 0 \\ A_0 + A_1 R, & -2 \leq R < 0 \end{cases} \quad (4.4)$$

where K_{op} represents the opening stress intensity factor and A_0, A_1, A_2, A_3 are the polynomial coefficients of Newman's crack opening function.

The result of NASGRO® equation (Equation (4.1)), the stress-ratio effect, is shown in Figure 4.6 and it was obtained by several experiments, where $\frac{\partial a}{\partial N}$ is in function of ΔK for different fitting of R (see Section 3.2, Equation (3.3)).

4.2.2.1 Pseudo-code

In this section, NASGRO® pseudo-code is presented with the same intent as Section 4.2.1.4. Here, the NASGRO equation is inserted in a *while* function to make it possible to determine the number of cycles to accomplish the imposed crack limits.

[2]Given by NASGRO® the values are $C = 5.448e^{-12}$, $m = 3.0$, $p = 0.5$ and $q = 0.75$

[3]This model was originally developed for a center crack in an infinite plate subjected to uniform stress, where the material deforms plastically in the wake of the crack as the crack advances [49]. The crack closure depends not only of R but also depends on the maximum stress level σ_{max} [50]

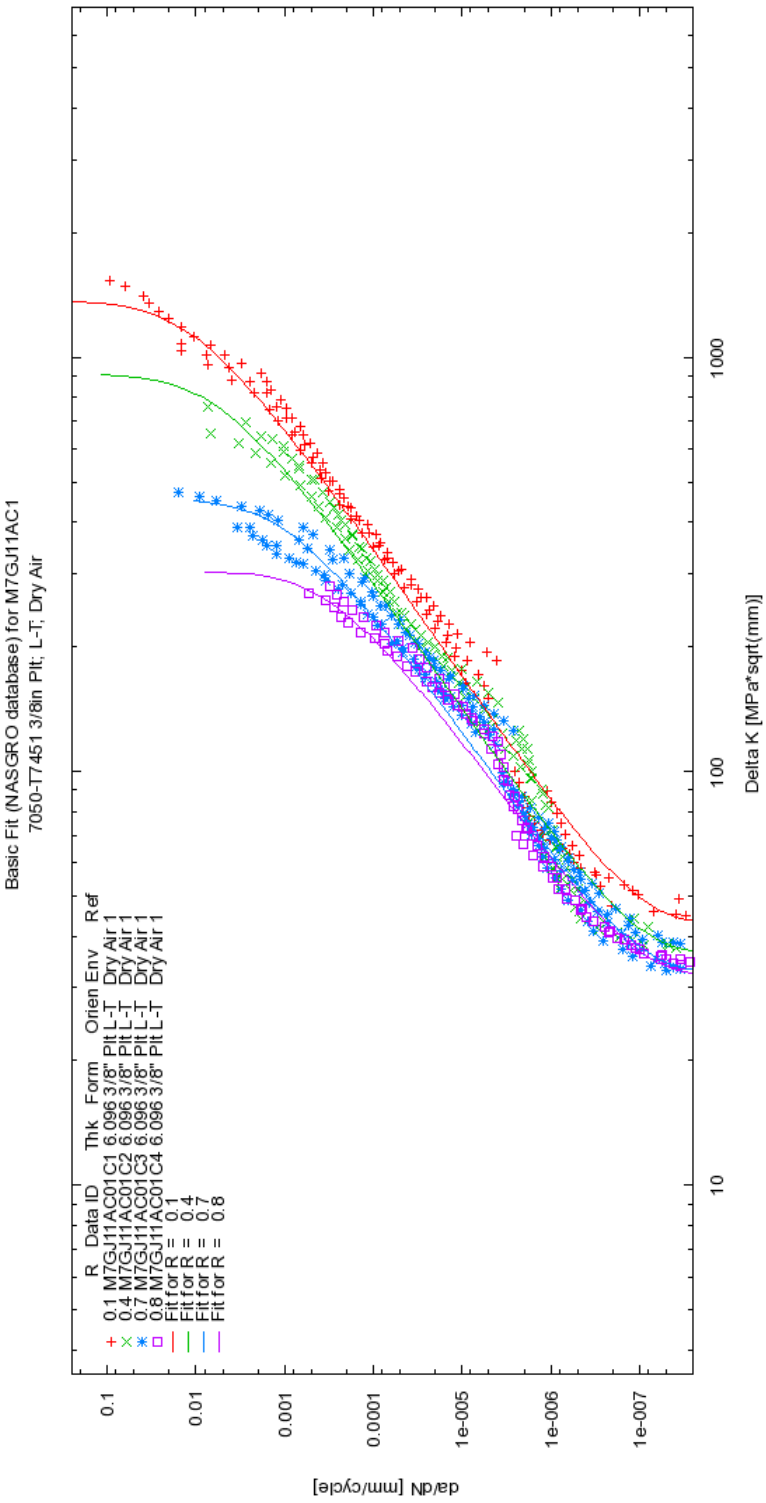

Figure 4.6: Material's NASGRO equation plot by NASGRO®.

Algorithm 2 NASGRO® Pseudo-code

1: **procedure** START($NASGRO$)
2: Set initial parameters (geometry, material, notch), stress conditions and crack limits
3: **while** crack limits are not achieved **do**
4: Calculate the number of cycles

$$\frac{\partial a}{\partial N} = C\left(\Delta K_{eff}\right)^{m} \frac{\left(1 - \frac{\Delta K_{th}}{\Delta K}\right)^{p}}{\left(1 - \frac{K_{max}}{K_c}\right)^{q}}$$

▷ Equation (4.1)

5: Print results

4.3 Numerical Results and Discussion

After the numerical procedure established, the numerical results of both softwares are presented as well as a brief discussion.

4.3.1 Abaqus® Numerical Results and Discussion

The FEM analysis main objective was the study of the stress intensity factor distribution along the crack width for different crack lengths. In this analysis the Stress Intensity Factor is calculated in Mode I with its loading condition perpendicular to the crack plane.
The stress value was defined as $\sigma = 430MPa$ that was explained in Section 4.2.1.1. The applied load was calculated by Equation (3.2) and the value of $P = 767.86N$ was obtained.
The initial considered parameters for initial notch assumed the value of $a = 0.1mm$ until it achieved half thickness, meaning that, the value of $a = 1mm$, for a crack length of $2c = 4mm$. The results are presented in Figure 4.7.

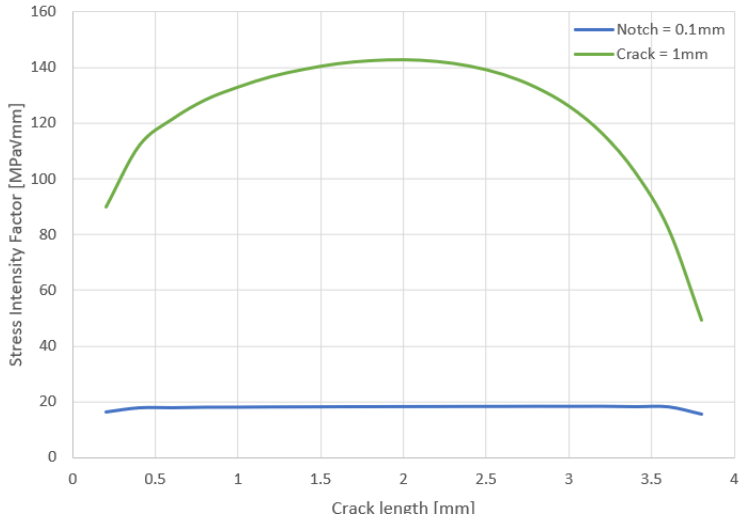

Figure 4.7: Stress intensity factor along crack length of the notch and the crack.

The plot represents the stress intensity factor in the notch when $a = 0.1mm$, and in the crack, $a = 1mm$. Here, it can be seen that the stress intensity factor is represented as a semi-elliptical

format.

The stress intensity factor assumes different values for each case, in the notch the stress is significantly lower when compared to the crack stress. The maximum value that is achieved in the crack tip in the middle of the crack length is equal to $K = 143.34MPa\sqrt{mm}$ and the minimum value located in the notch tip assumes a value of $K = 18.31MPa\sqrt{mm}$, for the applied stress of $430MPa$.

An abrupt change of values was registered in the borders of the crack length, Figure 4.8, that was omitted in the previous Figure 4.7 due to its irrelevance for the discussed case.

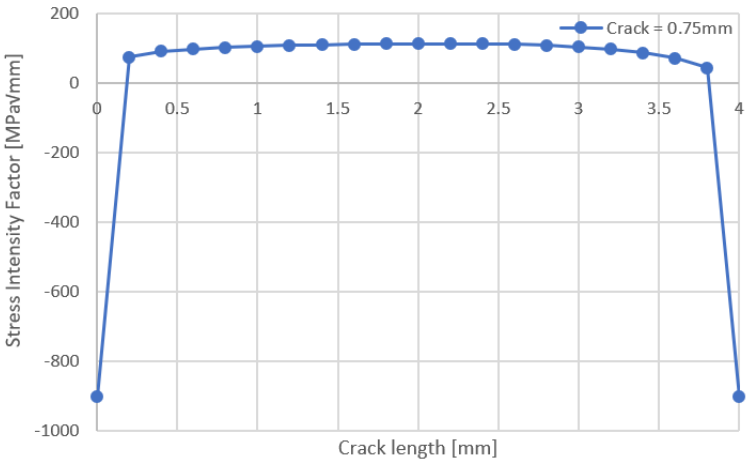

Figure 4.8: Representation of abrupt change of stress in the borders of crack length.

This event happened in all retrieved plots and it could be explained by the crack singularity, which is a theoretical concept that defines the crack tip with its radius ρ (Section 2.3.1) almost equal to zero, making the stress approach infinity.

A regular range of values for stress intensity factor was retrieved between the notch size and crack size. The values of $a = 0.25mm$, $a = 0.50mm$, $a = 0.75mm$ and $a = 1mm$ were used to assess the stress intensity factor evolution along the crack.

In Figure 4.9 the stress intensity factor along the crack depth for the aforementioned cases is presented, and as it can be seen from the notch until the crack, following the vertical line, there exists a smooth stress transition. The crack singularity effect is also removed from this plot for better visualization.

It is known that if the stress intensity factor is not inside the Paris region, the crack does not propagate through the specimen thickness. A small verification of the stress intensity value was made to assess if the values obtained would be in the Paris region. Figure 4.6 and Equation (4.5) were used and the results can be seen in Figure 4.10.

$$\Delta K = K_{max} - K_{min} \quad (4.5)$$

where K_{max} and K_{min} are obtained by Equation (2.15) for minimum and maximum stress obtained taking into account Equation (3.3).

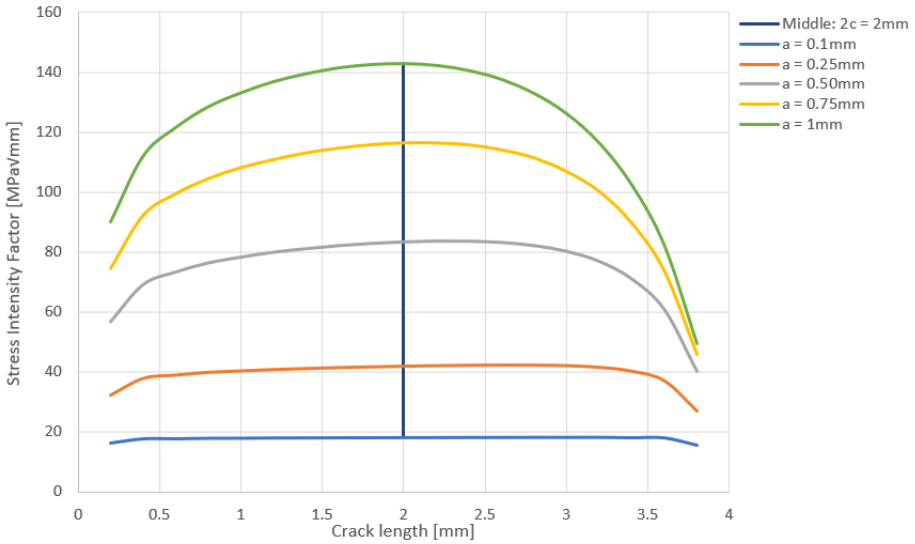

Figure 4.9: Stress intensity factor evolution along the crack depth.

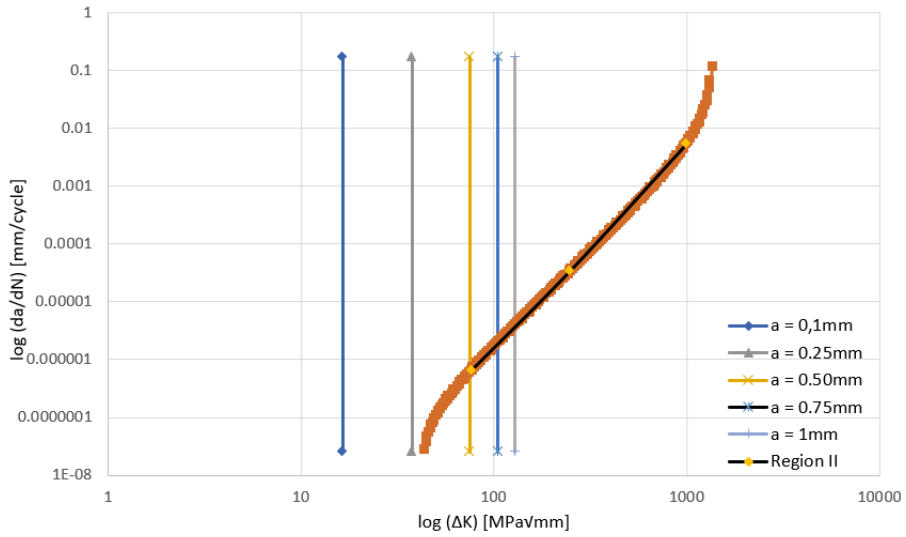

Figure 4.10: Comparison between the results and the material properties (Figure 4.6).

Each vertical line represents ΔK, which is calculated by Equation (4.5) for each crack depth obtained, and the line in orange represents the material properties retrieved by NASGRO® (same chart as Figure 4.6). The Region II of Paris Law is represented as a black line overlapped with the orange line.

It can be seen by this chart that the crack depth of $a = 0.1mm$ and $a = 0.25mm$ are in the Region I, this means, the notch will not propagate. However, the other values, which intersect the black line that represents Region II, are in the right domain.

Consequently, the initial defined parameters are not suitable to assess the crack propagation. However, the results obtained so far, are sufficient to calculate the more suitable initial notch size, being the value of $a = 0.50mm$ a good prediction. Figure 4.11 is a representation of the stress intensity factor evolution and the limit of Paris region.

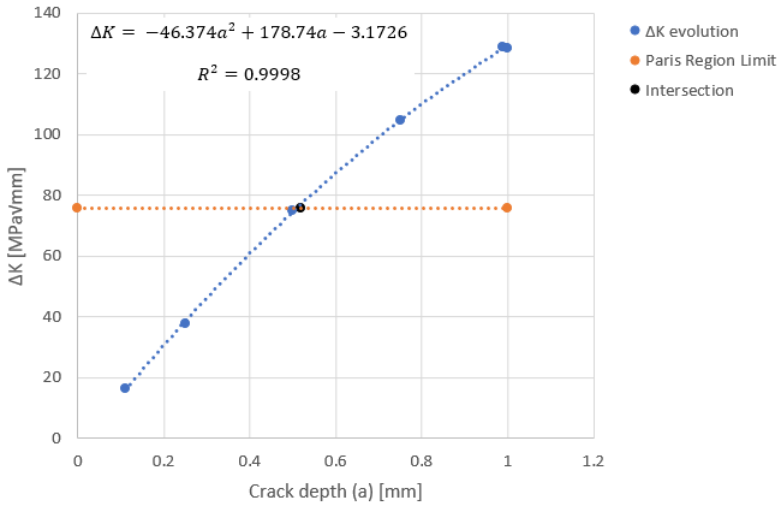

Figure 4.11: Stress intensity factor evolution as function as crack depth size intersected by the limit of the Paris region.

An intersection point is retrieved from Figure 4.11, which represents the minimum value of notch size that belongs to the Paris region. This point assumes the value of $a = 0.52mm$ and, as this value is already into the Paris region, it can be assumed that the notch dimensions of $4mm$ of length and $0.52mm$ of depth is a good prediction. In the same loading conditions and with this crack dimensions, it can be said that the crack is now able to propagate along the specimen depth.

As the notch represents more than $1/4$ of thickness, the crack limit was also adapted. As the main goal was to validate a non-destructive test method, a crack size until half thickness is a very small value, even for the experimental procedure. A total crack size of $1mm$ was chosen, which means that, for this specific case, since the notch size is assumed as $a = 0.52mm$, the crack size limit was imposed as $a = 1.52mm$.

In Figure 4.12 the crack in the values aforementioned is represented.

As can be seen in Figure 4.12, the crack is growing into the specimen thickness. In each stage of the crack the stress intensity factor is calculated and its representation along the crack length is presented in Figure 4.13 for the notch and final crack.

The maximum value of the stress intensity factor that is achieved in the crack tip in the middle of the crack length is equal to $K = 157.26MPa\sqrt{mm}$ and the minimum value located in the notch tip assumes the value of $K = 78.42MPa\sqrt{mm}$.

The aforementioned process was repeated in this stage: a comparison between the material properties and the values retrieved by Abaqus® was made, and the results are shown in Figure 4.14.

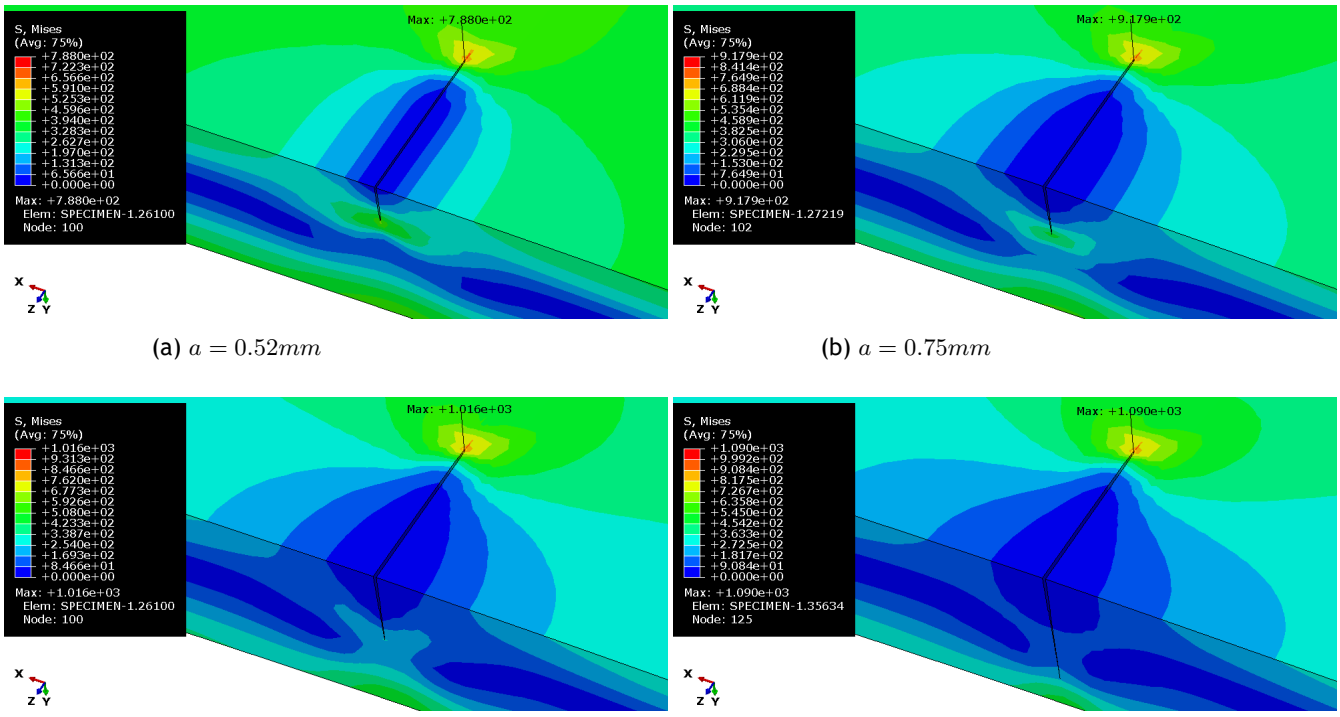

(a) $a = 0.52mm$ (b) $a = 0.75mm$

(c) $a = 1mm$ (d) $a = 1.52mm$

Figure 4.12: The different crack values across the depth.

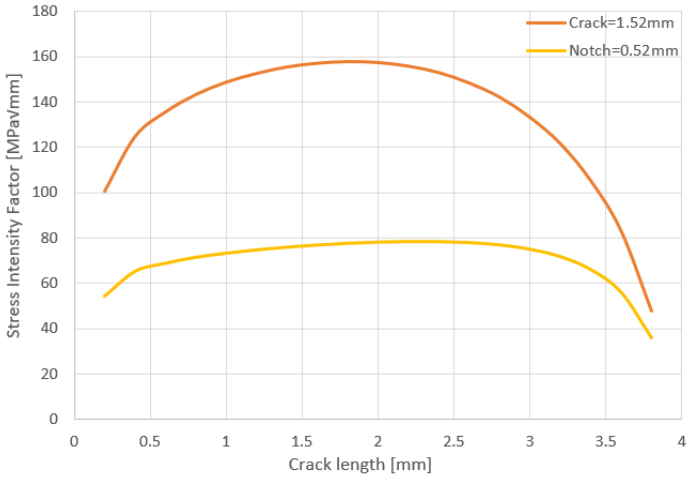

Figure 4.13: Stress intensity factor along crack length of the new notch and new crack.

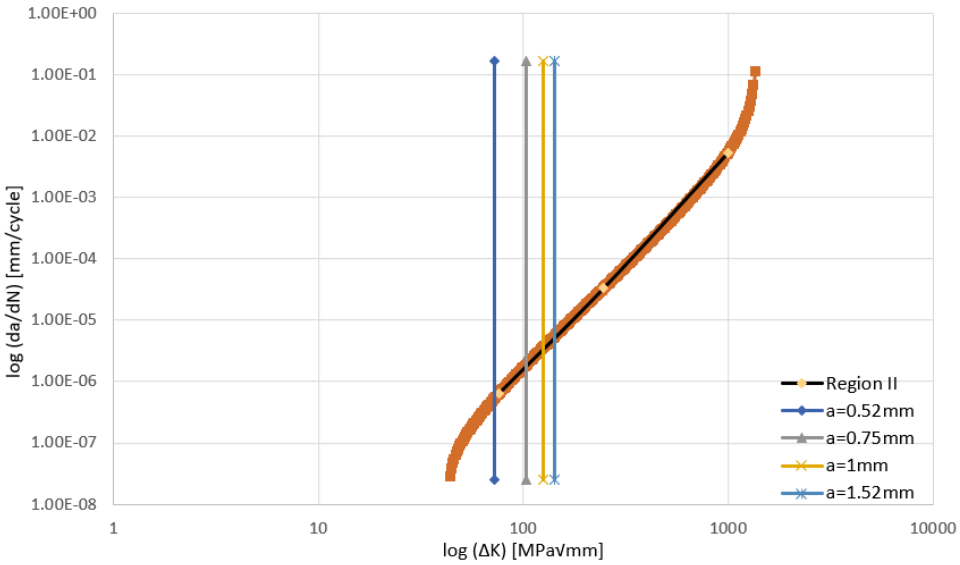

Figure 4.14: Comparison between the new results and the material properties (Figure 4.6).

A mathematical approach was performed having into consideration the results obtained by the previous method. The stress intensity factor evolution for these new values are presented in Figure 4.15.

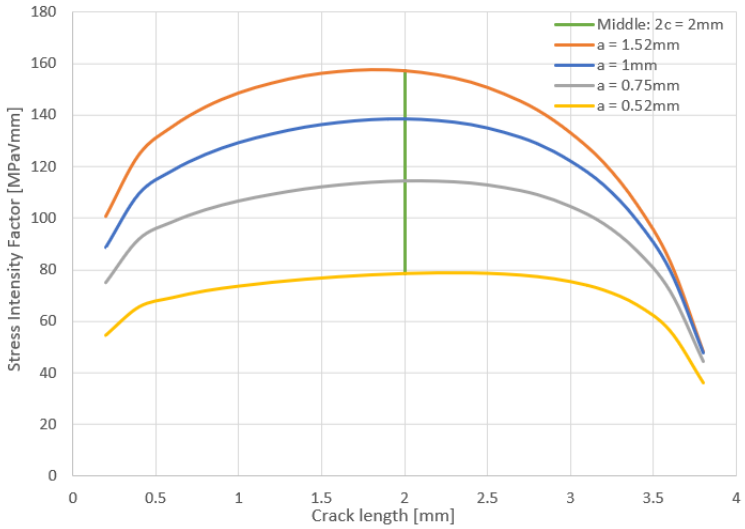

Figure 4.15: New stress intensity factor evolution along the crack depth.

Considering the stress distribution on crack tip given by Abaqus® in the middle of the crack length it is possible to determine by the variation of crack depth ∂a, the number of cycles that followed the propagation crack along thickness:

$$\frac{\partial a}{\partial N} = C(\Delta K)^m \quad (4.6)$$

The C and m parameters are obtained by NASGRO®, and the Paris Law, $\partial a/\partial N$, was calculated. The results are presented in Figure 4.16.

As can be seen in Figure 4.16a, the crack size is achieved in approximately 64700 cycles. The

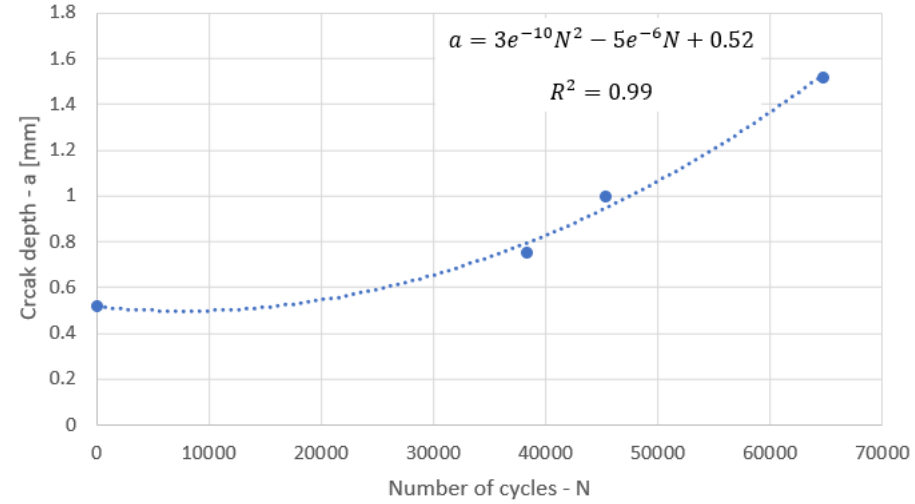

(a) ∂a as function as ∂N.

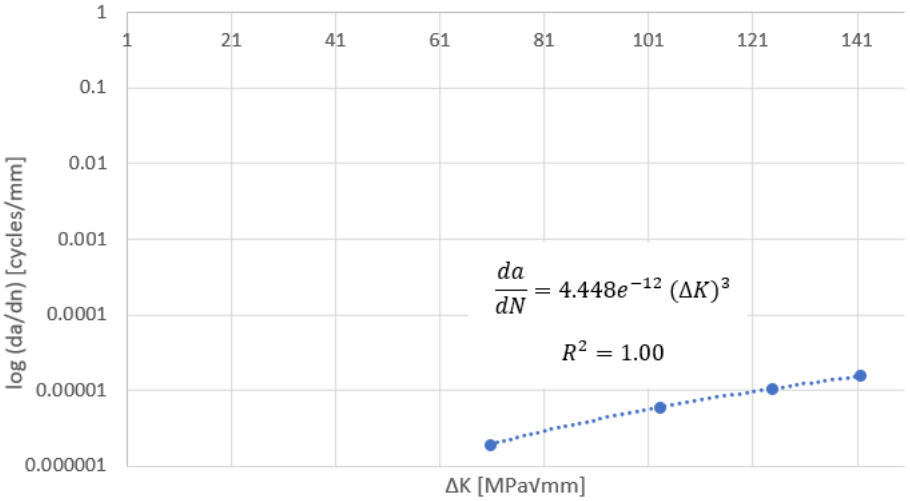

(b) $\partial a/\partial N$ as function as ΔK.

Figure 4.16: Obtained results using Abaqus® values and the Paris Law.

C and m parameters can be obtained by $\partial a/\partial N$ as function as ΔK, as represented in Figure 4.16b. As these parameters are material constants, the values retrieved should be the same as those obtained by NASGRO® (see Section 4.2.2), meaning this, $C = 5.448e^{-12}$ and $m = 3$, which is verified.

Other results can be retrieved by Abaqus® and they are also an assessment to verify if the crack is well represented. Related to Section 3.3, Figure 3.5, the cross section stress distribution of the specimen can be obtained with and without the crack.

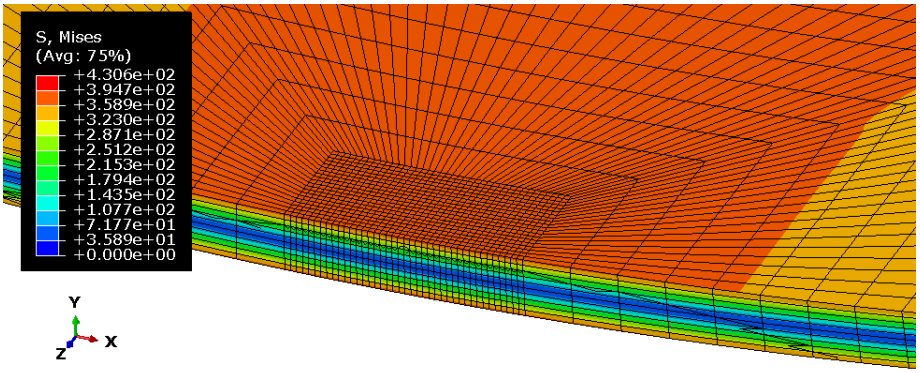

(a) Stress distribution without crack.

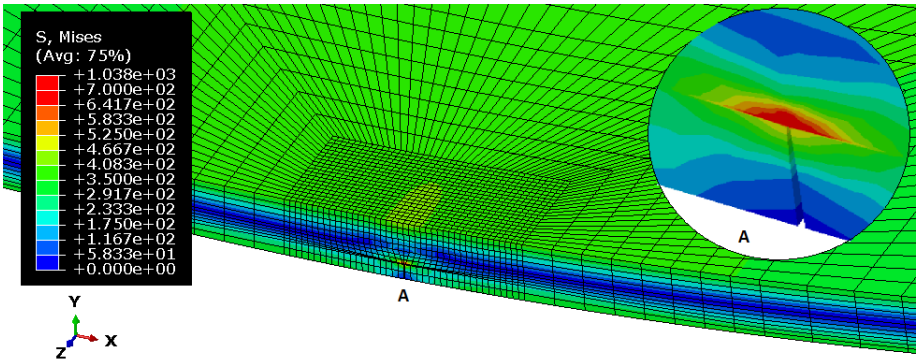

(b) Stress distribution with crack.

Figure 4.17: Stress distribution in the specimen cross section.

A brief distribution analysis of von Mises stress is applied to the crack plane and to the crack propagation plane, to obtain realistic results.

As said in Section 3.3, the neutral axis is stress-free, represented in blue in Figure 4.17a, however when the crack is induced, the neutral axis suffer a shift in the opposite direction of the crack, and it can also be detected that the maximum stress is seen in the crack-tip, represented in red in Figure 4.17b.

Also, Farahani *et al.* [10] successfully defined the concept of stress dead zone, in theoretical, experimental and computational analyses in cracked plates, having as basis the LEFM concepts. It was concluded that for 'all structural components carrying defects such as cracks, it is possible to delimit a zone where the stress field is very small, although the component is subjected to an external force system stressing it' [10]. Normally the dead zone has a triangular geometry, as can be seen in blue in Figure 4.18 and the red zone represents the maximum stress, associated to the crack-tip. For this dissertation case, these stress distributions are visible in the plane perpendicular of the crack propagation plane, denominated as crack plane.

The results from crack stress distribution are presented in Figure 4.19.

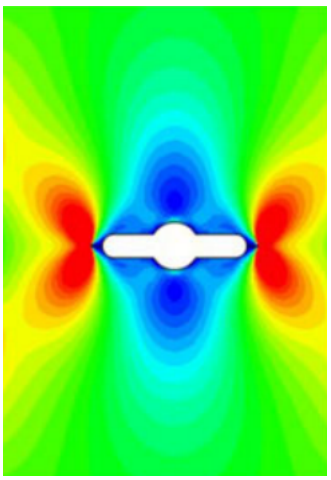

Figure 4.18: Crack stress distribution subjected to tensile stress perpendicular to the crack plane [10].

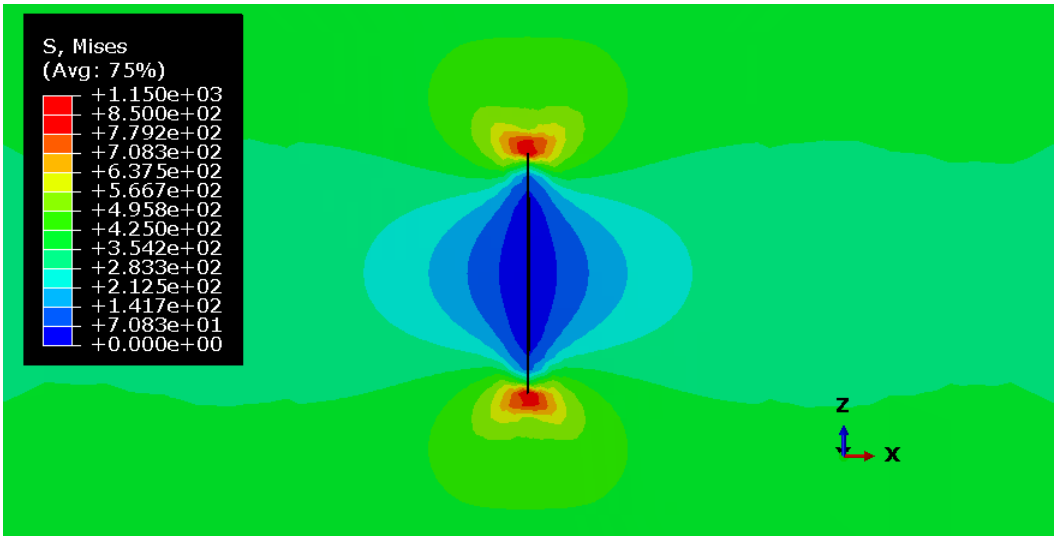

Figure 4.19: von Mises Stress distribution on crack plane along the y-direction.

The two previous figures show some similarities in the stress distribution. A high stress value, the red region, is well defined and located in the respective crack tips. The dead zone, the blue region, is also well defined and represents the lower stress.

Across the thickness, the stress distribution should be more intense in the crack tip, meaning this, when $a = 1.52mm$.

Kumar *et al.* [51] demonstrated a fatigue crack propagation in part-through cracked pipes by modelling a four-point bending test, where a semi-elliptical shape through the pipe thickness was visualized in the results. As the crack tries to propagate through thickness, the maximum stress should be located in that plane, and it should increase along the propagation crack growth direction, with an appearance of a maximum stress in that semi-elliptical zone.

Figure 4.20 represents the crack stress distribution in the thickness direction, which in this case is in the y-axis direction, and it can be seen that the semi-elliptical zone is also verified.

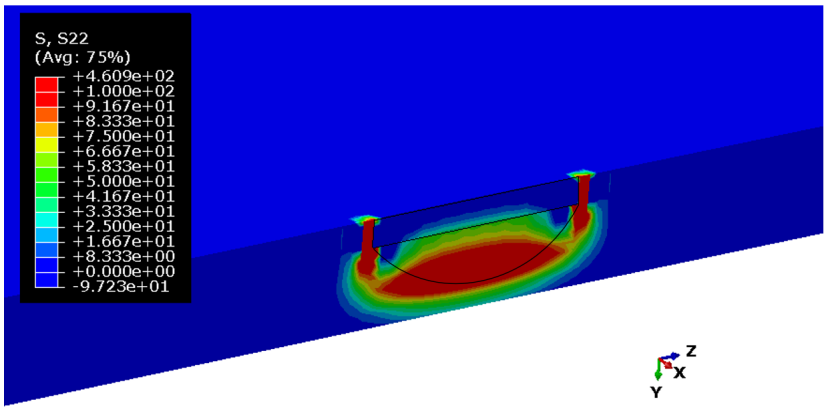

Figure 4.20: y-direction stress distribution on the propagation plane for the crack situation.

From Figure 4.21 it can be seen that the non-cracked surface assumes smaller stress values compared to the yield tensile strength, and as a result, it guarantees the material integrity. Values that exceed the yield tensile strength can only be verified in the crack zone.

The von Mises stress distribution in the crack is well defined, thereby the results could be presented as reliable results.

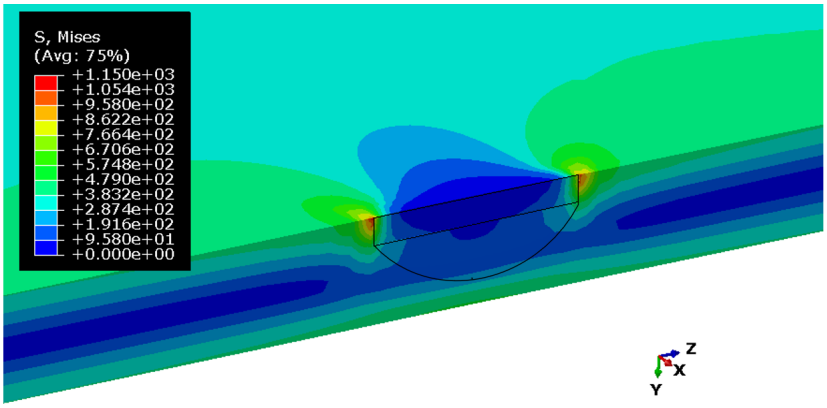

Figure 4.21: von Mises stress distribution along thickness.

From the retrieved results it can be said that the FEM represented the crack and its propagation growth according to the theoretical concepts and it was also possible to verify the stress intensity factor and how it is distributed in a crack propagation through thickness. The stress intensity increases with the crack propagation growth along the thickness achieving its minimum value in the notch and its maximum value in the crack tip.

4.3.2 NASGRO® Numerical Results and Discussion

The initial parameters requested by NASGRO® were initially chosen as it can be seen in Table 4.4.

Table 4.4: Initial conditions requested by NASGRO®

Parameter	
Thickness t	$2mm$
Width W	$100mm$
Crack offset B	$50mm$
Initial flaw size (depth) a	$0.52mm$
Initial a/c	0.26
Tension/compression stress $S0$	$0MPa$
Bending stress in the thickness $S1$	$430MPa$

The bending moment is represented as M, and the other parameters present in the Geometry SC30, Figure 4.5, are calculated below:

$$\frac{c}{Min(B, |W - B|)} = \frac{2}{Min(50, |100 - 50|)} = 0.04 < 0.95$$

The a/t parameter has to be between 0 and 0.95, which is verified:

$$a/t = \frac{0.52}{2} = 0.26$$

The initial a/c parameter was defined for an initial crack surface length of $2c = 4mm$, so:

$$a/c = \frac{0.52}{2} = 0.26$$

The crack limit is also a parameter that needs to be filled, which in this case was defined as $a = 1.52mm$ and c was left without restrictions.
With the initial conditions established, NASGRO® is able to determine how many cycles are necessary to achieve the limitation settings of crack dimension.
In this particular case, the crack achieved successfully the imposed final conditions at 12427 cycles, with its depth equal to $a = 1.51902mm$, its half-length $c = 6.16662mm$, and consequently the crack ratio of $a/c = 0.2463$.
Figure 4.22 shows the evolution of a and c along the number of cycles.

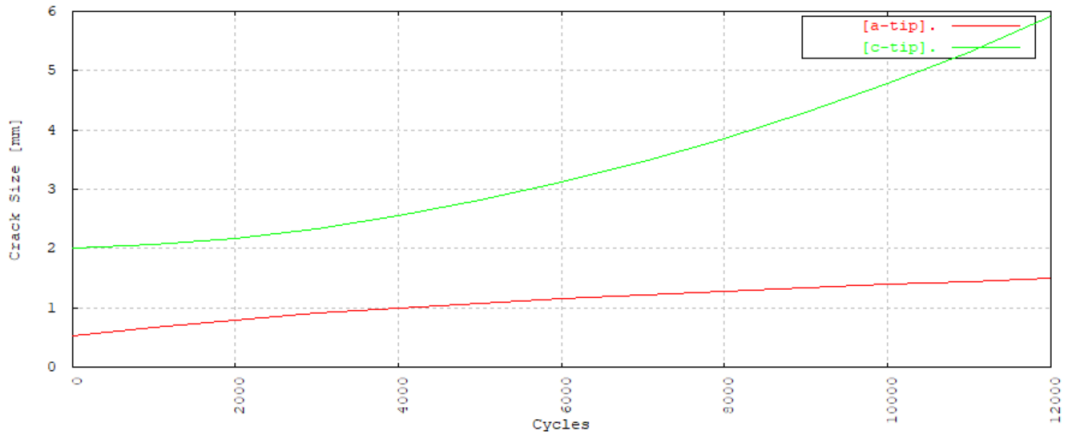

Figure 4.22: $\partial a/\partial N$ and $\partial c/\partial N$ from NASGRO®.

It can be observed that the a parameter starts with approximately $0.52mm$ and evolves to approximately $1mm$ at 4000 cycles and the c parameter starts with $2mm$ having an increasing

behaviour until final. The crack growth rate in the crack length direction and crack depth direction is different, however as can be detected an independent analysis of crack propagation in just one direction is impossible:

$$\begin{aligned} \Delta a = a_f - a_i = 1.51902 - 0.52 = 0.99902 \approx 1mm \\ \Delta c = c_f - c_i = 6.16662 - 2 = 4.17mm \\ \frac{\Delta a}{\Delta c} = 0.24 \end{aligned} \tag{4.7}$$

The difference between the initial and final dimensions is high, in relation to the initial crack dimensions and the specimen dimensions. The crack length grows $4.17mm$ for each side of a $100mm$ width specimen, and the crack depth grows until $1mm$ of a $2mm$ thickness specimen. From these results, it can be concluded that a four-point bending technique is a good method to investigate the crack depth propagation, having a small impact in the crack length growth.
A difference in the notch geometry can be noticed in both softwares. In NASGRO ® the notch geometry has a semi-elliptical format, however in Abaqus® a rectangular shape is chosen. Consequently, in the transversal direction, the notch has sharp edges in Abaqus®, which is not verified in NASGRO® and by that, the final results could be affected. Although the geometry is different, the notch dimensions are the same, where the length as $2c = 4mm$ and the depth as $a = 0.52mm$ were defined.
The crack growth in both directions are considered in NASGRO®, this means, the crack growth in depth and in length are calculated simultaneously, whilst in Abaqus® only the depth growth is considered. This situation could also originate the difference of final results between softwares.
In summary, both softwares are a possibility for assessing the crack propagation in a specimen, however the values acquired have a ratio of 5.21:

$$\frac{\text{Cycles calculated from Abaqus® data}}{\text{Cycles obtained from NASGRO®}} = \frac{64742}{12427} = 5.21 \tag{4.8}$$

which represents approximately 420% of difference. The value that corresponds to the most accurate choice can only be obtained by an experimental case, which should be the next approach. The experimental study is an important phase of development of this dissertation, not only to compare with the values obtained by the softwares, but also because it is an important study that allows assessing the behaviour of the material and all of the other parameters that are not accounted for in the numerical study.

Chapter 5

Conclusion

In this chapter the main conclusions of this dissertation are presented. Two sections are presented in order to describe the final remarks of this dissertation, where in the first section the achievements are described, having the conclusions from the results obtained in detail. In the second section some suggestions for future works are presented.

5.1 Achievements

The qualification of NDT processes from certain fatigue cracks dimensions was the study subject for this dissertation. The main focus with establishing the crack initial conditions and the final size crack was to determine the number of cycles in, which this specific crack evolved to its final form in a cracked specimen subjected to a four-point bending test. A sequential approach was chosen, starting with Abaqus® FEM software that was used to determine the stress intensity factor along the specimen thickness in the crack region, followed by a mathematical approach where the Paris Law was used and the number of cycles were retrieved. In the next step NASGRO® was used to estimate the number of fatigue cycles, and a comparison was made between the values obtained.

From Abaqus® software it was possible to conclude that the lower stress intensity factor is verified in the notch tip and the greater value is found in the crack tip. The results obtained by NASGRO® software allowed to conclude the good capability of the four-point bending test to restrict the crack propagation along the surface direction, having a reliable analysis in crack propagation along the depth. A mathematical approximation using the Paris Law and the results obtained by Abaqus® was made. A calculation of the number of cycles from the initial notch until the final crack dimension was performed to estimate the number of cycles necessary to grow the crack to a given size. Afterwards, in NASGRO®, the number of cycles were also obtained with the same conditions aforementioned. A difference of approximately 420% was verified between both softwares, witch is considered a significant value. However, this dissertation could be interpreted as a guide for the experimental work, which should be the next step to validate the results.

This study brought some information for a possible research on the SHM field. An aeronautical component that presents a crack with the same dimensions as studied in this dissertation, becomes a real challenge in the inspection processes. This type of crack configuration is almost impossible to detect by human eyes, due to the small crack lengths and due to the crack extension regarding the thickness direction. Achieving 75% of total component thickness, and having a superficial small notch length, this type of damage could be easily confused with simple superficial damage or even paint damage. The alarming part of the crack is not visible, so an alternative method has to be created. Many methods are already implemented in SHM, however, it is a field that deserves high concern and further development, especially in online monitoring of the complete aircraft structure.

5.2 Future Work

This section purpose is to suggest some future work that would complement and validate the results obtained in this dissertation.

The results provide some information that can be used in different applications, such as an experimental method. This, should be the first approach to consider for validation purposes, and the same configuration that was implemented should be used. Along with the experimental case, in the SHM field, a NDT process should be studied to find this type of damage. A full on-line monitoring method should be a preferential choice that should be implemented in all the critical aircraft parts. An easy and light implementation mechanism with a good precision should be the main characteristics that this process should present. The maintenance time and the human error could be decreased by this method of inspection, providing an improvement for aircraft safety as its main objective.

Further development such as numerical and experimental methods with variation of notch and crack dimensions should also be made. A comparison between the different cases should support and improve the NDT process, making it more precise and reliable for a vast range of cracks.

Bibliography

[1] R. Pinheiro Rulli, F. Dotta, and P. A. da Silva, "Flight tests performed by embraer with shm systems," in *Key Engineering Materials*, vol. 558. Trans Tech Publ, 2013, pp. 305–313. xiii, 7

[2] X. Katifes, "Structural analysis, fatigue analysis and optimization of aircraft wings," 2016. xiii, 8, 9

[3] B. Lourenço, "Damage tolerance design," Master's thesis, Dissertação de Mestrado em Engenharia Aeroespacial, Instituto Superior Técnico, 2010. xiii, 2, 9

[4] T. L. Anderson, *Fracture mechanics: fundamentals and applications*. CRC press, 2004. xiii, 1, 2, 11, 13, 14, 15, 16, 17, 18, 19

[5] N. E. Dowling, *Mechanical behavior of materials: engineering methods for deformation, fracture, and fatigue*. Pearson, 2012. xiii, 12, 14, 15, 16, 17, 19, 20, 21, 22, 25

[6] D. Broek, *The practical use of fracture mechanics*. Springer Science & Business Media, 1997. xiii, 11, 14, 21, 22

[7] D. Kopeliovich, "Flexural strength tests of ceramics," 2019. [Online]. Available: http://www.substech.com/dokuwiki/doku.php?id=flexural_strength_tests_of_ceramics xiii, 24

[8] J. Jordaan, "Four-point bending fatigue test specimen design by fea," *R&D Journal*, vol. 34, pp. 1–8, 2018. xiii, 10, 25, 26

[9] A. Preisler, C. Steenbock, and K.-U. Schröder, "Crack diagnosis of metallic profiles based on structural damage indicators," in *Journal of Physics: Conference Series*. IOP Publishing, 2015. xiii, 26, 27

[10] B. V. Farahani, S. Eslami, F. Q. de Melo, P. J. Tavares, and P. M. Moreira, "Concept of stress dead zone in cracked plates: Theoretical, experimental, and computational studies," *Fatigue & Fracture of Engineering Materials & Structures*, 2019. xiv, 45, 46

[11] M. M. P. Data, "Aluminum 7050-t7451 (7050-t73651)," 2019. [Online]. Available: http://www.matweb.com/search/datasheet_print.aspx?matguid=142262cf7fbc4c83917ca5c3d17df1ed xv, 30

[12] D. W. Wragg, *Speed in the Air*. Osprey Publishing, 1974. 1

[13] M. S. Fright, "Isogrid design handbook," 1973. 1

[14] FAA, "Advisory Circular - Guide for Developing a Receiving Inspection System for Aircraft Parts and Material," *AFS-300*, 12/12/2005. 2

[15] G. Zhao, C. Kwan, Z. Ren, and B. Ayhan, "Wireless health monitoring of an aircraft wing," 01 2004. 2, 6, 8

[16] P. Foote, "New guidelines for implementation of structural health monitoring in aerospace applications," *SAE International Journal of Aerospace*, vol. 6, no. 2013-01-2219, pp. 525–533, 2013. 5

[17] C. Keulen, B. Rocha, M. Yildiz, and A. Suleman, “Structural health monitoring using lamb wave based piezoelectric networks and phased array solutions,” 2014. 5

[18] NASA. (2019) Nondestructive evaluation. [Online]. Available: https://www.nasa.gov/centers/wstf/supporting_capabilities/nondestructive_evaluation/index.html 6, 7

[19] G. de Oliveira Prado, A. K. Tamba, F. Dotta, L. C. Vieira, R. P. Rulli, G. R. Silva, and J. Moreira, “Further results of lamb waves approach to assess corrosion damage in an aeronautical aluminum alloy,” 2016. 6

[20] F. Dotta and L. B. Ceresetti, “Evaluation of the lamb waves approach to detect simulated damage in orthogonal plane of the sensor network surface for corrosion detection application,” in *Health Monitoring of Structural and Biological Systems 2013*, vol. 8695. International Society for Optics and Photonics, 2013, p. 86951L. 6

[21] J. D. Achenbach, “Quantitative nondestructive evaluation,” *International Journal of Solids and Structures*, vol. 37, no. 1-2, pp. 13–27, 2000. 6

[22] K. Worden, G. Manson, and D. Allman, “Experimental validation of a structural health monitoring methodology: Part i. novelty detection on a laboratory structure,” *Journal of Sound and Vibration*, vol. 259, no. 2, pp. 323–343, 2003. 6

[23] C. Wölfinger, F. Arendts, K. Friedrich, and K. Drechsler, “Health-monitoring-system based on piezoelectric transducers,” *Aerospace science and technology*, vol. 2, no. 6, pp. 391–400, 1998. 6

[24] J. Cai, L. Qiu, S. Yuan, L. Shi, P. Liu, and D. Liang, “Structural health monitoring for composite materials,” in *Composites and their applications*. IntechOpen, 2012. 6

[25] G. Qi, H. Lei, R. Geng, and P. Jing, “Recent developments of aircraft nondestructive evaluation based on advanced sensor techniques,” in *Seventeenth world conference on nondestructive testing*, 2008, pp. 1951–1958. 6

[26] T. Nelligan and C. Calderwood, “Introduction to eddy current testing,” 2019. [Online]. Available: https://www.olympus-ims.com/en/eddycurrenttesting/ 6

[27] InfraTec., “Active thermography as a process for non-destructive testing,” 2019. [Online]. Available: https://www.infratec-infrared.com/thermography/non-destructive-testing/ 7

[28] D. Dynamics, “What is laser shearography,” 2019. [Online]. Available: https://www.dantecdynamics.com/products-and-services/what-is-laser-shearography 7

[29] N. Mrad, “State of development of advanced sensor systems for structural health monitoring applications,” in *Proceedings of the NATO RTO AVT-144 Workshop on Enhanced Aircraft Platform Availability Through Advanced Maintenance Concepts and Technologies, Vilnius, Lithuania*. Citeseer, 2006, pp. 3–5. 7

[30] D. N. Alleyne and P. Cawley, “The interaction of lamb waves with defects,” *IEEE transactions on ultrasonics, ferroelectrics, and frequency control*, vol. 39, no. 3, pp. 381–397, 1992. 7

[31] S. Beeby, G. Ensell, M. Kraft, and N. White, “Mems mechanical sensors. artech house,” *Inc. Boston, London*, pp. 85–112, 2004. 8

[32] E. Bruhn, “Analysis and design of flight vehicle structures,” *Tri-state offset company*, pp. B1, C13, 1973. 8, 9, 10, 11

[33] S. Habib, W. B. Yousuf, T. Mairaj, and S. Khalid, “Fatigue crack growth prediction on a310 aircraft wing using static analysis,” in *2017 14th International Bhurban Conference on Applied Sciences and Technology (IBCAST)*. IEEE, 2017, pp. 71–75. 8, 12, 13

[34] A. Payne, “The fatigue of aircraft structures,” *Engineering Fracture Mechanics*, vol. 8, no. 1, pp. 157–203, 1976. 10

[35] A. D’Amore, G. Caprino, P. Stupak, J. Zhou, and L. Nicolais, “Effect of stress ratio on the flexural fatigue behaviour of continuous strand mat reinforced plastics,” *Science and Engineering of Composite Materials*, vol. 5, no. 1, pp. 1–8, 1996. 10, 25

[36] W. Schütz and P. Heuler, “A review of fatigue life prediction models for the crack initiation and propagation phases,” in *Advances in fatigue science and technology*. Springer, 1989, pp. 177–219. 12

[37] S. Suresh, *Fatigue of materials*. Cambridge university press, 1998. 12

[38] A. N. V. da Silva, “Analytical modeling of the stress-strain distribution in a multilayer structure with applied bending,” Master’s thesis, IST - Instituto Superior Técnico, 2010. 21

[39] J. J. Schubbe, “Plate thickness variation effects on crack growth rates in 7050-t7451 alloy thick plate,” *Journal of Materials Engineering and Performance*, vol. 20, no. 1, pp. 147–154, 2011. 23

[40] L. Molent, Q. Sun, and A. Green, “Characterisation of equivalent initial flaw sizes in 7050 aluminium alloy,” *Fatigue & Fracture of Engineering Materials & Structures*, vol. 29, no. 11, pp. 916–937, 2006. 23

[41] R. M. Guedes, *Creep and fatigue in polymer matrix composites*. Woodhead Publishing, 2010. 23

[42] C. Garcia, T. Lotz, M. Martinez, A. Artemev, R. Alderliesten, and R. Benedictus, “Fatigue crack growth in residual stress fields,” *International Journal of Fatigue*, vol. 87, pp. 326–338, 2016. 24, 34

[43] M. Baxter, R. Pullin, K. M. Holford, and S. Evans, “Detection of fatigue crack growth in aircraft landing gear, 4 point bend test specimens,” in *Key Engineering Materials*, vol. 293. Trans Tech Publ, 2005, pp. 193–200. 24

[44] A. Standard, “D6272-10,” *Standard test method for flexural properties of unreinforced and reinforced plastics and electrical insulating materials by four point bending. ASTM International*, 2010. 24

[45] ASTM, “E647-00,” *Standard Test Method for Measurement of Fatigue Crack Growth Rates*, vol. 100, 2000. 29

[46] X. Fengmei, L. Fuguo, F. Juan, L. Jiang, and Y. Zhanwei, “Experiments and simulations on tensile properties and fracture toughness of 7050-t7451 aluminum alloy hole specimens,” *Rare Metal Materials and Engineering*, vol. 42, no. 9, pp. 1767–1772, 2013. 29

[47] J. J. Schubbe, “Fatigue crack propagation in 7050-t7451 plate alloy,” *Engineering Fracture Mechanics*, vol. 76, no. 8, pp. 1037–1048, 2009. 30

[48] S. Mettu, V. Shivakumar, J. Beek, F. Yeh, L. Williams, R. Forman, J. McMahon, and J. Newman Jr, "Nasgro 3.0: A software for analyzing aging aircraft," 1999. 36

[49] D. Tong and X. Wu, "Analysis of crack opening stresses for center-and edge-crack tension specimens," *Chinese Journal of Aeronautics*, vol. 27, no. 2, pp. 291–298, 2014. 36

[50] M. A. Meggiolaro and J. T. P. De Castro, "On the dominant role of crack closure on fatigue crack growth modeling," *International Journal of Fatigue*, vol. 25, pp. 843–854, 2003. 36

[51] P. Kumar, V. K. Sahu, P. Ray, and B. Verma, "Modelling of fatigue crack propagation in part-through cracked pipes using gamma function," *Mechanics, Materials Science & Engineering Journal*, p. 77, 2016. 46